European Journal of Medicinal Chemistry 289 (2025) 117402

Contents lists available at ScienceDirect

European Journal of Medicinal Chemistry

journal homepage: www.elsevier.com/locate/ejmech

Research paper

Furazanopyrazine-based novel promising anticancer agents interfering with the eicosanoid biosynthesis pathways by dual mPGES-1 and sEH inhibition

Gianluigi Lauro [a,1], Michela Aliberti [a,1], Mauro De Nisco [b], Silvana Pedatella [c], Giacomo Pepe [a], Manuela Giovanna Basilicata [d], Maria Giovanna Chini [e], Katrin Fischer [f], Robert K. Hofstetter [f], Oliver Werz [f], Maria Grazia Ferraro [g], Marialuisa Piccolo [h], Carlo Irace [h], Anella Saviano [i], Pietro Campiglia [a], Alessia Bertamino [a], Carmine Ostacolo [a], Tania Ciaglia [a], Michele Manfra [b,*], Giuseppe Bifulco [a,**]

[a] Department of Pharmacy, University of Salerno, Via Giovanni Paolo II 132, Fisciano, 84084, Italy
[b] Department of Health Sciences, University of Basilicata, Viale dell'Ateneo Lucano, Potenza, I-85100, Italy
[c] Department of Chemical Sciences, University of Napoli Federico II, Via Cintia 4, I-80126, Napoli, Italy
[d] Department of Advanced Medical and Surgical Sciences, University of Campania "Luigi Vanvitelli", P.zza L. Miraglia 2, 80138, Naples, Italy
[e] Department of Biosciences and Territory, University of Molise, C.da Fonte Lappone, Pesche, 86090, Italy
[f] Department of Pharmaceutical/Medicinal Chemistry, Institute of Pharmacy, Friedrich Schiller University Jena, Philosophenweg 14, Jena, 07743, Germany
[g] Department of Molecular Medicine and Medical Biotechnologies, School of Medicine and Surgery, University of Naples, Via Domenico Montesano 49, Naples, 80131, Italy
[h] BioChem Lab, Department of Pharmacy, School of Medicine and Surgery, University of Naples, Via Domenico Montesano 49, Naples, 80131, Italy
[i] ImmunoPharmaLab, Department of Pharmacy, School of Medicine and Surgery, University of Naples Federico II, Via Domenico Montesano 49, 80131, Naples, Italy

ARTICLE INFO

Keywords:
Inflammation
mPGES-1
sEH
Furazanopyrazine
Virtual screening
Cancer

ABSTRACT

We report the identification of a new set of compounds based on the furazanopyrazine core interfering with eicosanoid biosynthesis and acting as potentially effective anti-inflammatory and anticancer agents. Based on our previous promising results on a set of furazanopyrazine-based compounds against the microsomal prostaglandin E_2 synthase-1 (mPGES-1) enzyme, we here identified derivatives with improved pharmacokinetic properties by replacing the ester moiety with a more stable ether group.

A focused virtual library of 1×10^4 molecules was built and screened against mPGES-1 through molecular docking experiments, leading to the selection of 10 candidates for synthesis and biological evaluation. Several molecules were found to inhibit mPGES-1 and, among them, two items featured IC_{50} values in the low micromolar range. Additional computational studies on the collection of synthesized compounds demonstrated that compound **3b**, previously emerged as an mPGES-1 inhibitor, interfered with soluble epoxide hydrolase (sEH) activity, thus emerging as a valuable dual mPGES-1/sEH inhibitor. The pharmacokinetic features of the most potent compounds were accurately estimated. Unfortunately, poor outcomes were obtained for **3b**; on the other hand, compound **7e** exhibited promising mPGES-1 inhibition and excellent pharmacokinetic profile, demonstrating that the novel furazanopyrazine-based items with ether moiety possess improved pharmacokinetic properties compared to the ester-based compounds reported in our previous study. Additionally, the anticancer properties of **7e** and **7d**, the latter emerged as the most active mPGES-1 inhibitor, were evaluated and both compounds showed promising activities against HCT-116 human colorectal cancer (CRC) cells.

These findings highlight the furazanopyrazine core as a promising scaffold for disclosing new anti-inflammatory drugs with the ability to inhibit targets belonging to arachidonic acid cascade.

* Corresponding author.
** Corresponding author.
E-mail addresses: michele.manfra@unibas.it (M. Manfra), bifulco@unisa.it (G. Bifulco).
[1] These authors contributed equally to this work.

https://doi.org/10.1016/j.ejmech.2025.117402
Received 16 December 2024; Received in revised form 13 February 2025; Accepted 14 February 2025
Available online 18 February 2025

1. Introduction

Prostaglandin E_2 (PGE_2) is a crucial mediator of inflammation since it is involved in various pathological diseases, including immune surveillance, inflammation, cell death, proliferation, and angiogenesis [1]. Cyclooxygenases (COXs) act together with terminal PG synthases (PGES, especially mPGES-1, mPGES-2, and cPGES) to produce PGE_2 from arachidonic acid (AA). In contrast to the constitutively expressed isoforms mPGES-2 and cPGES, mPGES-1 is an inducible membrane-bound isoform implicated in a number of acute and chronic diseases [2]. Therefore, mPGES-1 inhibition is a viable strategy in the therapy of chronic inflammation-related illnesses, such as colorectal cancer (CRC), and aids in the development of novel medications that limit the inflammation-induced production of PGE_2 [3].

Although several mPGES-1 inhibitors have been reported so far, only a few compounds, such as ISC 27864, GS-248, LY3031207, and LY3023703, have advanced to the clinical trial stage [2]. In recent years, the roles that epoxyeicosatrienoic acids (EETs) and soluble epoxide hydrolase (sEH) play in inflammation and pain have been widely investigated. The biological effects of EETs are lost when they are broken down into their corresponding dihydroxyeicosatrienoic acids (DHETs or DiHETrEs) by soluble epoxide hydrolase (sEH) [4]. Furthermore, various studies have demonstrated that sEH inhibitors lower plasma concentrations of nitric oxide metabolites and pro-inflammatory cytokines, and support the resolution of inflammation by promoting the synthesis of lipoxins [5,6].

We have been extensively involved in the discovery of several mPGES-1 and sEH inhibitors featuring different chemical scaffolds over the past ten years [7–15]. Among them, we recently reported that the 9*H*-indeno[1,2-*b*][1,2,5]oxadiazolo[3,4-*e*]pyrazin-9-one core is an intriguing framework for the development of mPGES-1 inhibitors with putative anti-inflammatory and antitumor properties [10]. In this field, furazanopyrazine-containing molecules represent promising hit/lead compounds for the development of drugs that can be crucial in treating serious illnesses, such as inflammatory disorders and cancer [16]. However, the most potent furazanopyrazine-based mPGES-1 inhibitors developed by our research group featured an ester function, that prompted us to investigate the possibility of replacing this unstable moiety with different chemical functions while preserving their interesting mPGES-1 inhibitory activity.

In this work, based on this chemical scaffold, novel synthetic derivatives with improved pharmacokinetic properties were developed and evaluated for their inhibitory activity against mPGES-1 and sEH. The promising results reported here were achieved through a well-structured workflow encompassing computational research, chemical synthesis, and biological assessment of the most promising hit compounds.

2. Results and discussion

The workflow designed to identify furarazopyrazine-based compounds as multi-target anti-inflammatory agents is illustrated in Fig. 1. The subsequent paragraphs offer an in-depth explanation of each step involved in this process.

2.1. Preliminary in silico evaluation of substituted furazanopyridine compounds

Furazanopyrazine has emerged as a promising scaffold for the development of new small molecules targeting mPGES-1. In details, in a previous study, we identified 9*H*-indeno[1,2-*b*][1,2,5]oxadiazolo[3,4-*e*]pyrazine-9-one derivatives, obtained by inserting aryl ester substituents at the central core, showing a significant inhibitory activity against mPGES-1 [10]. Starting from these compounds, we performed optimization studies to develop novel derivatives with an enhanced pharmacological profile targeting mPGES-1. This led us to investigate the pharmacokinetic profile and biological activity of compounds **3a-c**, **7a-e**, **8a-e**, **12**–**13** (see Schemes 1–3, respectively).

mPGES-1, a membrane protein dependent on glutathione (GSH), is structured as a homotrimer with three equivalent monomers, here

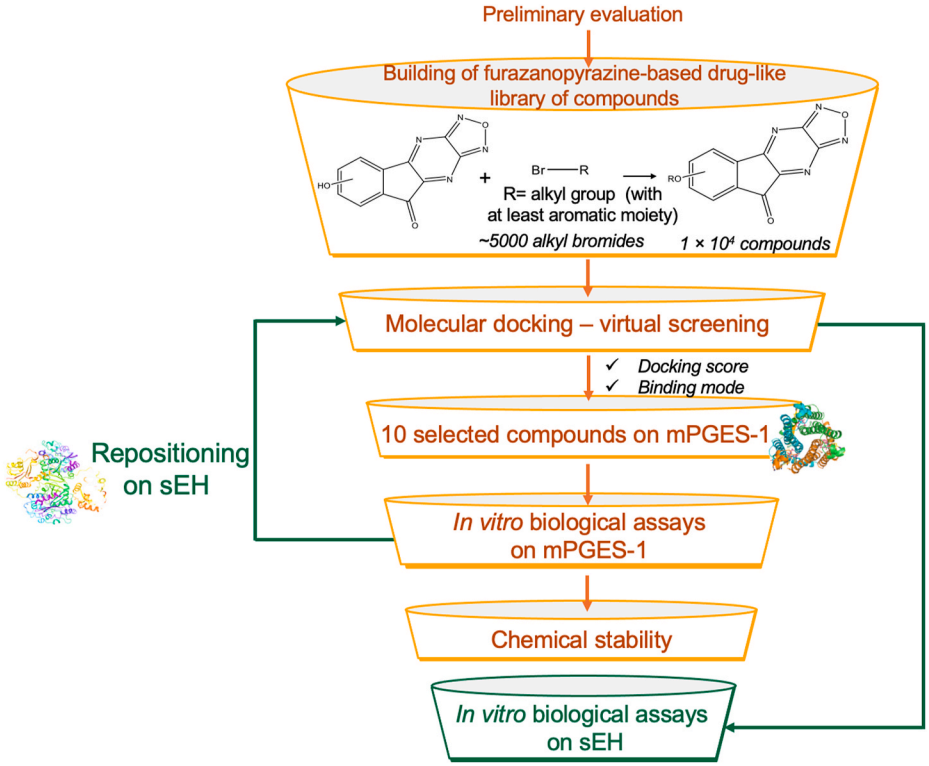

Fig. 1. The workflow for the development of novel furazanopyrazine-based compounds.

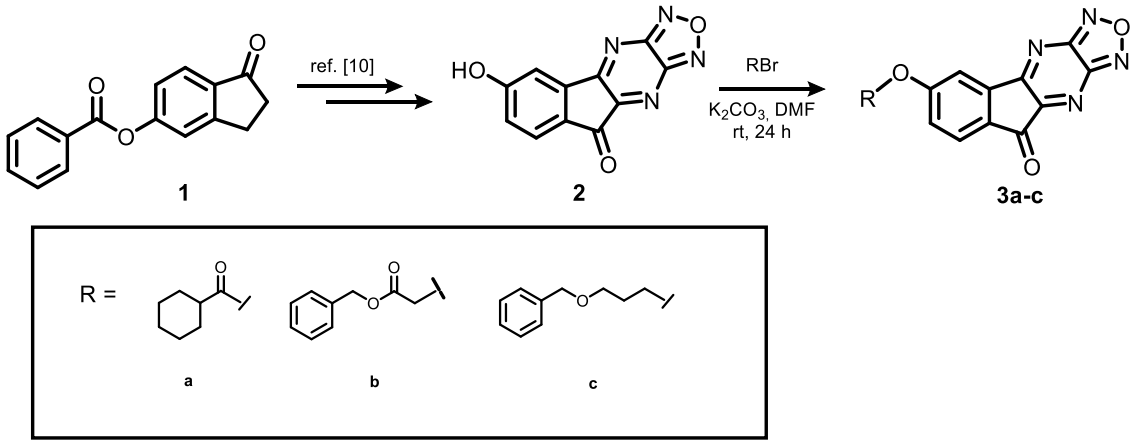

Scheme 1. Synthetic pathway for compounds **3a-c**.

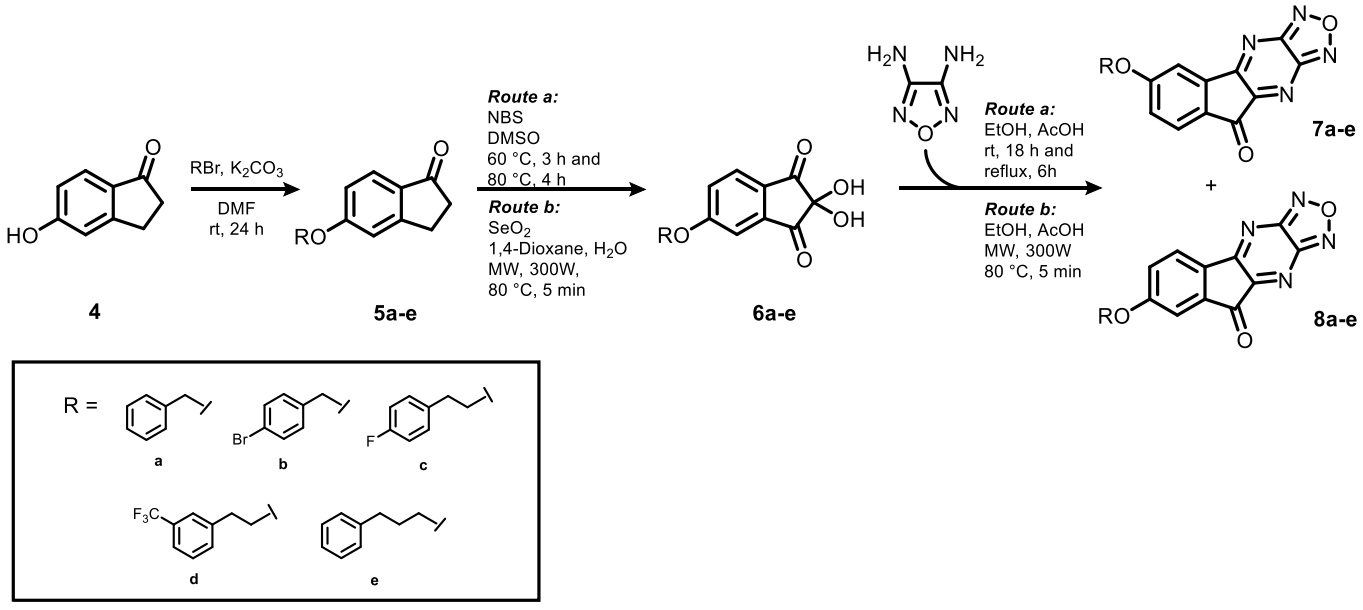

Scheme 2. Synthetic pathway for compounds **7a-e** and **8a-e**.

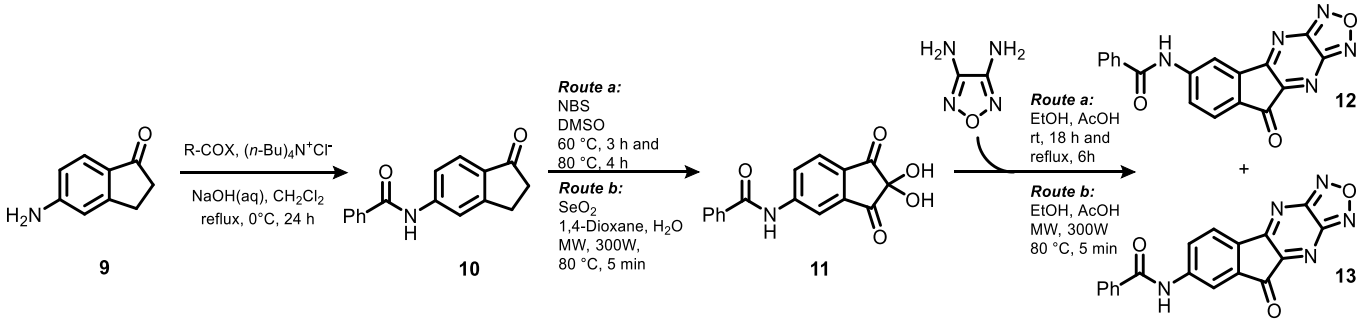

Scheme 3. Synthetic pathway for compounds **12** and **13**.

named A, B, and C. Each monomer has an active site in the membrane-spanning region, which includes a GSH cofactor molecule and distinct residues originating from adjacent monomers [17]. Owing to the diverse chemical properties and spatial orientations of these residues, various regions within the mPGES-1 binding site can be identified at the interface between two adjacent monomers (e.g., A and B) and comprised of residues with different chemical features. Primarily, a groove is present between the GSH binding site and a molecular region near the cytoplasmic segment of the protein, consisting of both aromatic (B:Phe44, B: His53) and polar (B:Asp49) residues. The GSH cofactor is located in a deep cavity, which exhibits a distinct U-shaped conformation resulting from strong interactions between its terminal carboxylate groups and

the positively charged residues of mPGES-1 (B:Arg38, A:Arg73). In the cytoplasmic domain of the protein, a binding groove is identified between helix 1 of chain B and helix 4 of chain A, which includes polar (A:Gln134), aliphatic (B:Val24), and aromatic (B:Tyr28) residues. Based on these insights into the mPGES-1 active site, our initial goal was to determine the importance of an aromatic moiety on the substituent at positions 6 or 7 of the scaffold. Specifically, we replaced the acyl ester of the **BEO1** (Fig. 2), which previously emerged as one of the most active hit compounds [10], with a cyclohexanecarboxylate group, resulting in compound **3a**, which was then investigated through computational studies and biological assays.

Molecular docking experiments indicated that the absence of an aromatic group at position 6 led to the loss of critical interactions with A:Tyr130, resulting in reduced inhibitory activity (Fig. 3). This was corroborated by biological assays, in which the compound inhibited mPGES-1 activity by only 30 % at a concentration of 10 μM. These results highlighted the necessity of retaining the aromatic ring at this position to ensure potent inhibitory activity against mPGES-1.

Furthermore, to enhance the chemical stability of the compounds and improve their pharmacokinetic properties, we investigated the profile of **BEO1**, which contains an ester group easily susceptible to hydrolysis. To optimize its pharmacokinetic features, we substituted the aryl ester substituent with a more stable benzamidic group. Molecular docking analysis revealed that, while the central scaffold is oriented towards amino acids A:Arg126 and A:Ser127, the substituent at positions 6 or 7 for regioisomers **12** and **13** (according to the chemical synthesis procedure, see Schemes 1-3) failed to proficiently interact with residues towards the GSH binding pocket and, specifically, to establish van der Waals interactions with A:Tyr130, likely due to the planar feature of the amide bond (Fig. 4). As predicted, both synthesized compounds **12** and **13** did not exhibit sufficient inhibitory activity on mPGES-1 (see Schemes 1-3).

Consequently, we considered replacing the ester group with an ether function to overcome these limitations. In particular, we evaluated the ability of compounds **7a** and **8a** to inhibit mPGES-1 through *in silico* studies and biological assays. Computational studies revealed that these compounds occupy the binding site of mPGES-1 in a promising way, as they were able to interact with the key amino acids (Fig. 5) and, in particular, to establish edge-to-face π-π interactions with B:His53. The biological evaluation confirmed the predicted inhibitory activity against mPGES-1 by compound **7a**. Remarkably, preliminary pharmacokinetic investigations assessing the chemical stability of compound **7a** in gastric fluid demonstrated the favorable profile of this derivative when compared with **BEO1** (see *2.6 Microsomal Stability*).

2.2. Building of a library of furazanopyrazine based-compounds and virtual screening against mPGES-1

Based on the preliminary data obtained, we built a new virtual library of furazanopyrazine compounds by replacing the original ester functional group with a more stable ether moiety with the final aim of obtaining new derivatives with enhanced pharmacokinetic properties. Considering synthetic accessibility (see *2.3 Chemistry*), we generated two libraries of 5.8×10^4 molecules each, by combining approximately 5000 commercially available alkyl bromides, containing at least an aromatic ring, with 6-hydroxy-9*H*-indeno[1,2-*b*][1,2,5]oxadiazolo[3,4-*e*]

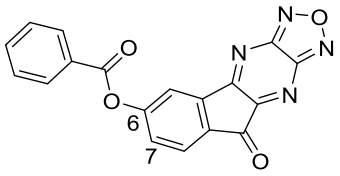

Fig. 2. 2D structure of **BEO1**.

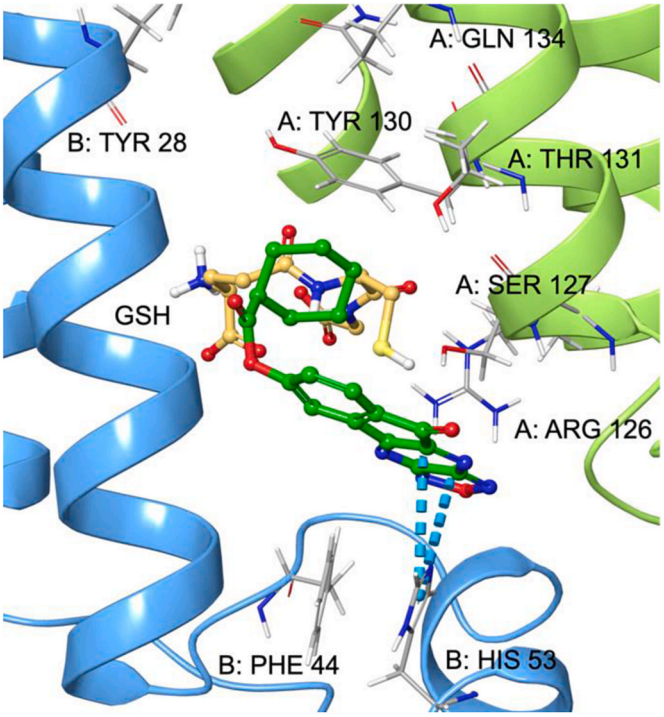

Fig. 3. Binding mode of **3a** (coloured according to atom type: C green, O red, N blue) in the binding site of mPGES-1 (chains A and B are shown as green and blue ribbons, respectively) in the presence of the cofactor GSH (coloured according to atom type: C faded orange, O red, N blue, S yellow, polar H grey). *π-π* stacking interactions are represented as dotted blue lines. (For interpretation of the references to colour in this figure legend, the reader is referred to the Web version of this article.)

pyrazin-9-one and 7-hydroxy-9*H*-indeno[1,2-*b*][1,2,5]oxadiazolo[3,4-*e*]pyrazin-9-one chemical cores (see *2.3 Chemistry*), respectively (using CombiGlide software, see Experimental section). Subsequently, pharmacokinetic filters were applied to exclude compounds with unfavorable predicted ADME profile (see Experimental section). The resulting library was subjected to virtual screening for evaluating potential mPGES-1 (PDB ID: 4BPM [18]) inhibition through molecular docking experiments. The most promising compounds were identified through an in-depth analysis of their binding mode and interaction pattern with the receptor site of interest.

Starting from the structural information of mPGES-1 described above, compounds that complied with the following key interactions were selected:

- interactions with B:Tyr28, B:Phe44, B:His53;
- polar contacts with A:Arg126, A:Ser127, A:Thr131, B:Gln36, B:Asp49;
- π-π interactions with A:Tyr130, a key residue interacting with GSH as a cofactor.

From this virtual screening, compounds **3b, 3c**, **7b-e**, and **8b-e** were identified as the most promising candidates through docking analysis and were selected for the subsequent chemical synthesis step.

The analysis of docking poses showed a similar binding mode for the selected compounds. As reported in Fig. 6, the chemical core occupied the active site of mPGES-1, establishing two π-π stacking interactions with B:Tyr28 and A:Tyr130, which indicated a good accommodation within the GSH binding site, while the aryl group was directed toward the amino acid B:Phe44 and B:His53.

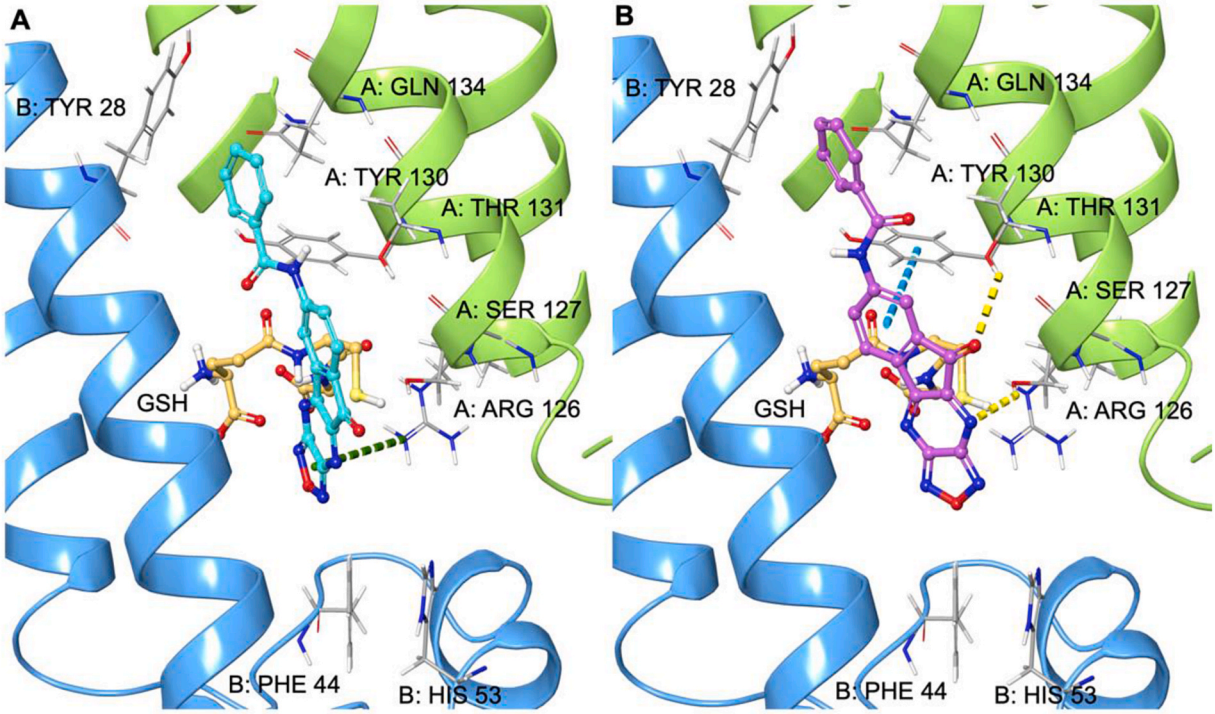

Fig. 4. Binding mode of **12** (A) (coloured according to atom type: C cyan, O red, N blue) and **13** (B) (coloured according to atom type: C faded plum, O red, N blue) in the mPGES-1 (chains A and B are shown as green and blue ribbons, respectively) binding site in the presence of the cofactor GSH (coloured according to atom type: C faded orange, O red, N blue, S yellow, polar H grey). Hydrogen bonds are represented as dotted yellow lines, π-π stacking interactions are represented as dotted blue lines and π-cation in green. (For interpretation of the references to colour in this figure legend, the reader is referred to the Web version of this article.)

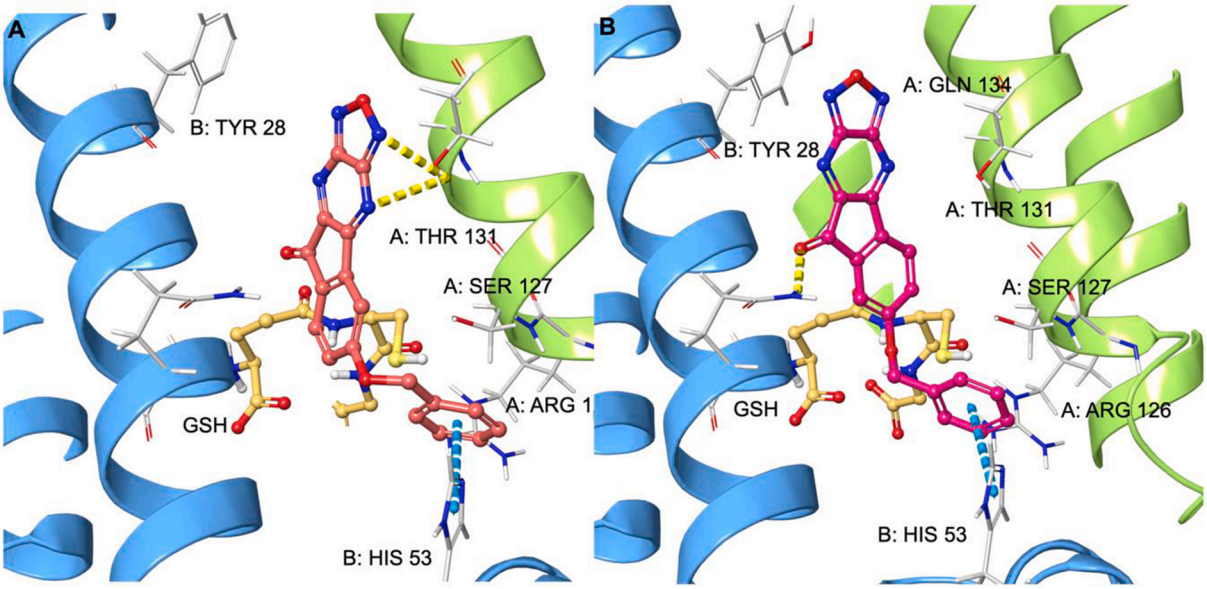

Fig. 5. 3D representation of the binding mode of **7a** (A) (coloured according to atom type: C faded red, O red, N blue) and **8a** (B) (coloured according to atom type: C magenta, O red, N blue) in the mPGES-1 (Chains A and B are shown as green and blue ribbons, respectively) binding site in the presence of the cofactor GSH (coloured according to atom type: C faded orange, O red, N blue, S yellow, polar H grey). Hydrogen bonds are represented as dotted yellow lines, π-π stacking interactions are shown as dotted blue lines. (For interpretation of the references to colour in this figure legend, the reader is referred to the Web version of this article.)

2.3. Chemistry

Substituted analogues **3a-c** were obtained, driving the Bratton's protocol [19] with appropriate modification [10] (Scheme 1). In detail, the synthesis of derivative **2** started from electrophilic bromination with *N*-bromosuccinimide of the freshly prepared benzoyl derivate of the commercially available 5-hydroxy-1-indanone, followed by oxidation using dimethyl sulfoxide. Condensation of the latter intermediate *gem*-diol with furazan-3,4-diamine in a mixture of ethanol and acetic acid afforded two 4- and 5-substituted regioisomers tetracycles in a ratio of 0.88:1, respectively. The two isomers were readily separated and purified by silica gel chromatography, followed by ester cleavage of

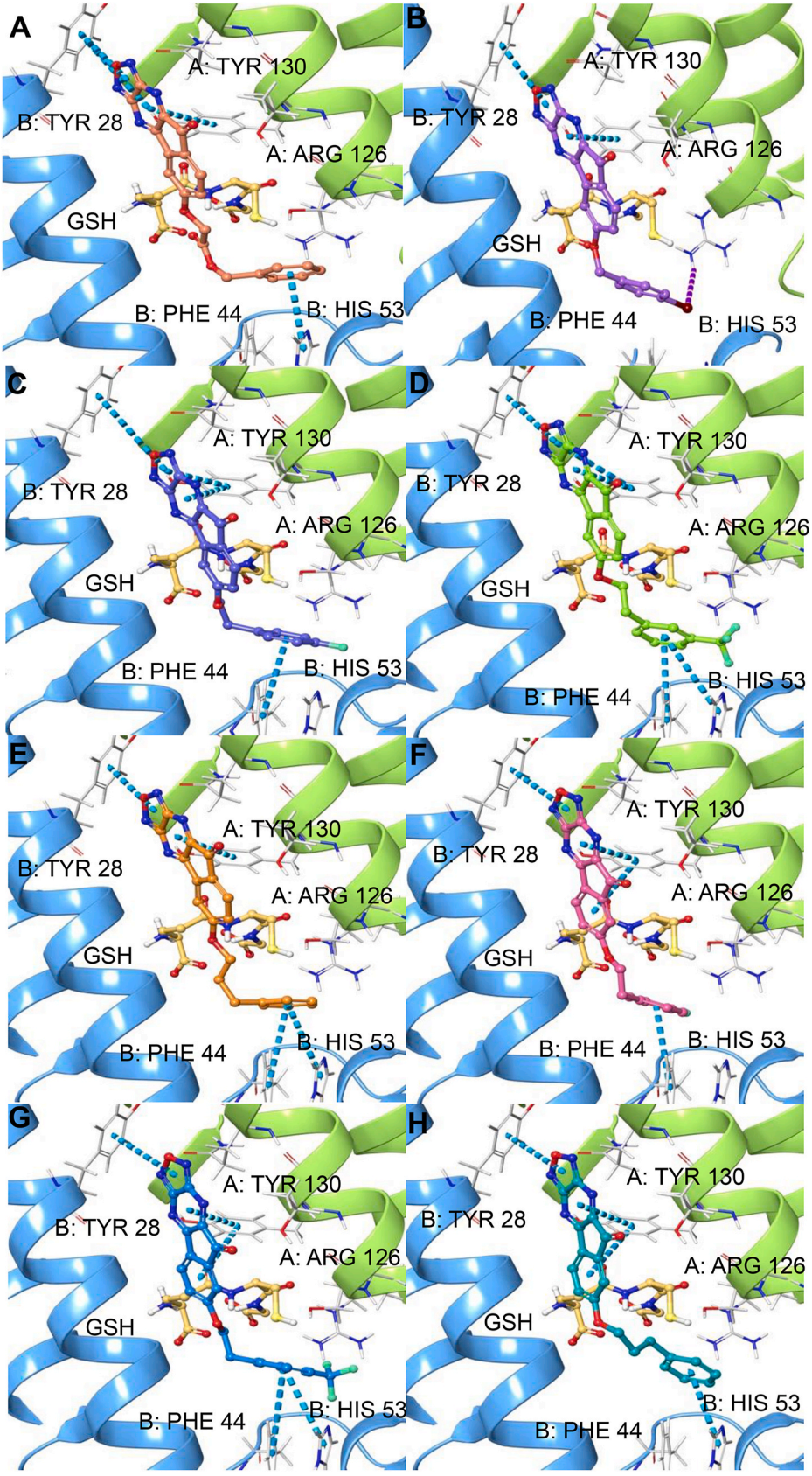

(caption on next page)

Fig. 6. Binding mode of **3b** (A) (coloured according to atom type: C faded red-orange, O red, N blue), **7b** (B) (coloured according to atom type: C violet, O red, N blue, Br dark purple), **7c** (C) (coloured according to atom type: C faded blue, O red, N blue, F teal), **7d** (D) (coloured according to atom type: C light green, O red, N blue, F aqua green), **7e** (E) (coloured according to atom type: C orange, O red, N blue), **8c** (F) (coloured according to atom type: C pink, O red, N blue, F aqua green), **8d** (G) (coloured according to atom type: C azure, O red, N blue, F aqua green), **8e** (H) (coloured according to atom type: C teal green, O red, N blue) in the mPGES-1 (chains A e B are shown as green and blue ribbons) binding site in the presence of the cofactor GSH (coloured according to atom type: C faded orange, O red, N blue, S yellow, polar H grey). π-π stacking interactions are represented as dotted blue lines while halogen bonds are shown as dotted violet lines. (For interpretation of the references to colour in this figure legend, the reader is referred to the Web version of this article.)

5-substituted tetracycle with sodium thiophenolate in MeOH/THF (1:1), which produced the corresponding phenol **2** in 95 % yield.

It is noteworthy that the phenolic derivative is useful for the introduction of additional moieties. Namely, nucleophilic substitution was employed to add a range of alkyl groups to the phenolic function.

Thus, the treatment of **2** with alkylbromide in DMF under basic conditions (K_2CO_3) at room temperature for 24 h afforded compounds **3a-c** [20].

At that point, we approached a different pathway where steps of protection and corresponding deprotection of the benzoyl group were escaped through the use of intermediates **5a-e** prepared from indanone **4**. In this way, compounds **7a-e**, **8a-e**, **12** and **13** (Schemes 2 and 3) were obtained in satisfactory yields. Instead, the new route was not successful for compounds **3a-c**, maybe because the reaction conditions were not compatible with the alkyl chain. We accomplished the same results when the conversion of **5a-e** in the corresponding tetracycles analogues was carried out with a microwave-assisted procedure [21]. Indeed, as reported in Table 1, compounds **7a-e**, **8a-e**, **12** and **13** were achieved with no very impressive improvement in yields but with very interesting reduced reaction times [from 31 h (7 h + 24 h) to 10 min (5 min +5 min)].

2.4. In vitro evaluation of the inhibitory activity of the selected compounds on mPGES-1

To test the effects of the compounds on inhibition of mPGES-1 activity, we employed a cell-free enzyme activity assay using microsomes of interleukin-1β-stimulated A549 cells as mPGES-1 source and PGH_2 (20 μM) as substrate; formed PGE_2 was measured as mPGES-1 product using RP-HPLC and MK886 served as reference drug [22,23]. Among the selected test compounds that were screened at a concentration of 10 μM, the compounds **7c**, **7d**, and **8d**, carrying a 4-fluoro-phenylethyl or 3-trifluoromethyl-phenylethyl residues in 6- or 7-position of the 9*H*-indeno [1,2-*b*][1,2,5]oxadiazolo[3,4-*e*]pyrazin-9-one core, were most efficient and inhibited mPGES-1 activity by approximately 70 %, similar as the reference drug MK886 (10 μM) (see Table S2). Also, compounds **7b**, **7e** and **8c** with 4-bromophenylmethyl, phenylpropyl, or 4-fluoro-phenylethyl moieties inhibited mPGES-1 activity at 10 μM by >50 %, albeit apparently less efficient as the former three derivatives (see Table S2). All other compounds had some minor activity, with <45 % inhibition of mPGES-1. More detailed concentration-response studies with the most promising candidates revealed IC_{50} values of 1.0 ± 0.2 μM and 3.5 ± 0.7 μM for **7d** and **8d**, respectively (see Fig. S58).

Table 1
Yields (%) of the compounds **7a-e**, **8a-e**, **12** and **13** were obtained by applying the classical method and Microwave-assisted procedures.

Compound	Classic Method Yield (%)	MW Methods Yield (%)
7a	27	32
7b	35	40
7c	35	37
7d	25	26
7e	36	39
8a	23	24
8b	24	26
8c	25	26
8d	18	19
8e	21	22
12	13	15
13	12	12

2.5. Computational studies and biological evaluation of the subset of furazanopyrazine derivatives on soluble epoxide hydrolase (sEH)

Given the encouraging results obtained for mPGES-1 inhibition, we decided to evaluate the activity of these compounds against the soluble epoxide hydrolase (sEH), a key target involved in the AA cascade and which has recently captured our interest due to its important role in inflammation and cancer [11,12,14,24]. Specifically, sEH is a homodimeric enzyme including, in each monomer, a phosphatase site in the N-terminal domain and a hydrolase site in the C-terminal domain, which is involved in the metabolization of epoxyeicosatrienoic acids (EETs) [4]. While the phosphatase site is still poorly understood, the hydrolase site has been well investigated. It takes the form of a long "L"-shaped hydrophobic tunnel containing the amino acid residues Tyr383, Tyr466, and Asp335, which are part of catalytic triad [25,26]. Tyrosine phenolic groups have been shown to be involved in the mechanism of action of enzyme by polarizing the epoxide group of the natural substrate, while aspartate makes a nucleophilic attack with its carboxyl group.

Various inhibitors of the sEH enzyme were developed over the years, including alkylureas, which have key structural features for interaction with this enzyme [27]:

- a hydrogen bond acceptor group (e.g., a carbonyl group of urea or amide) that interacts with Tyr383 and Tyr466, mimicking the oxygen of the epoxide in natural substrates;
- a hydrogen bond donor group, such as the NH of an amide or urea, capable of establishing a bond with Asp335.

Based on this information, we screened the compounds selected on mPGES-1 against sEH by molecular docking experiments. Careful analysis of docking poses revealed that compound **3b** possessed promising characteristics as a potential sEH inhibitor (Fig. 7). Indeed, among the

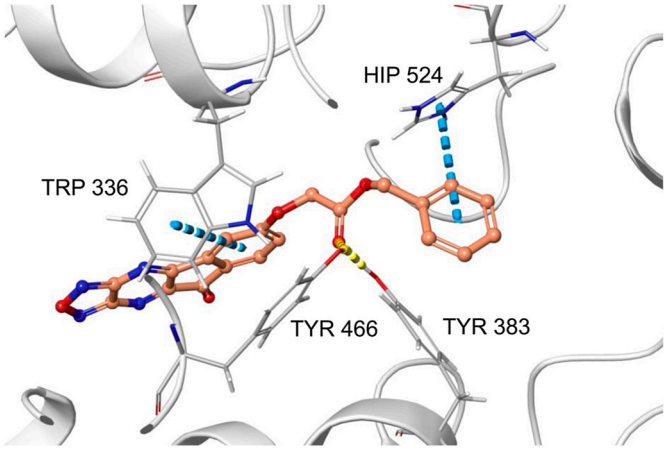

Fig. 7. 3D representation of **3b** (coloured according to atom type: C faded red-orange, O red, N blue) in the hydrolase binding site of sEH (represented as grey ribbons). Hydrogen bonds are shown as dotted yellow lines, π-π stacking interactions are represented as dotted blue lines. (For interpretation of the references to colour in this figure legend, the reader is referred to the Web version of this article.)

tested compounds, we observed that the carbonylic moiety of **3b** acted as a hydrogen bond acceptor, interacting with the amino acids Tyr383 and Tyr466, which are part of the catalytic triad of the enzyme. In addition, the two aromatic rings of compound **3b** occupied the hydrophobic region of the binding pocket, by establishing interactions with amino acids His524 and Trp336, which contribute to the inhibitory activity.

The results from the docking studies with sEH encouraged us to test experimentally if compound **3b** could inhibit sEH activity. We employed a well-established cell-free activity assay for sEH using purified human recombinant sEH as enzyme source and 3-phenyl-cyano(6-methoxy-2-naphthalenyl)methyl ester-2-oxiraneacetic acid (PHOME) as substrate; AUDA (12-[[(tricyclo[3.3.1.13,7]dec-1-ylamino)carbonyl]amino]-dodecanoic acid) was used as reference drug [28]. As shown in Fig. 8, compound **3b** yielded a comparable inhibitory activity (± SEM) at 10 μM against sEH (48 ± 10 %) as against mPGES-1 (44 ± 7 %).

2.6. Microsomal Stability

Based on the promising data obtained for the screened furazanopyrazine-based compounds, we investigated step-by-step the pharmacokinetic features of a small set of selected compounds. Specifically, we focused on evaluating the chemical stability of the starting compound **BEO1** and the most potent inhibitors of mPGES-1, particularly those synthesized with higher reaction yields. This strategy enabled a comparative analysis of the chemical stability of all derivatives substituted at the 6-position of the core scaffold.

In this context, human liver microsomes (HLM) are subcellular fractions derived from the liver's endoplasmic reticulum, obtained through differential high-speed centrifugation. These fractions contain various enzymes like CYPs, flavin-monooxygenase, carboxylesterases, epoxide hydrolase, and UGTs, making HLM a preferred *in vitro* model for drug metabolism studies. The incubation process requires NADPH or an NADPH regenerating system, and UDGPA and alamethicin are needed for UGT activity determination. HLM are favored due to their simplicity, cost-effectiveness, long-term storage, and suitability for high-throughput screening [29–32]. For these reasons, in this study we evaluated the hepatic stability of test compounds after incubation with HLMs. In our assay, we monitored the loss of the test compounds over time through CYP-UGT-mediated metabolic pathways.

The extent of microsomal clearance allowed the determination of different pharmacokinetic parameters such as *in vitro* $t_{1/2}$, $CLint_{in\ vitro}$ and $CLint_{in\ vivo}$. *In vitro* $t_{1/2}$ and CLint of test compounds after liver microsomes incubation were calculated according to the "*well stirred*" model [33].

As expected, our results first highlighted that compound **3b** is categorized as having high clearance. On the other hand, compounds **BEO1** and **7c** were categorized as having intermediate clearance (Table 2) [34]. Among the tested compounds with low *in vivo* calculated intrinsic hepatic clearance, **7e** and **7b** demonstrated the best stability after hepatic microsomal incubation.

2.7. In vitro bioscreens for anticancer activity

mPGES-1 has increasingly been recognized as a critical target for cancer suppression due to the role of PGE_2 as a bioactive lipid mediating various biological effects, including those related to malignancy, particularly in colorectal cancer (CRC) [35,36]. Compounds **7d** and **7e**, which exhibited promising inhibitory effects on mPGES-1 and demonstrated good pharmacokinetic profiles, were evaluated for their antiproliferative activity on human HCT-116 cells, a widely used preclinical *in vitro* model for human CRC in numerous biomedical studies [37]. As depicted in Fig. 9, the cell survival index indicates moderate antitumor effects for test compounds, with IC_{50} values in the low micromolar range (Table 3). Notably, compound **7e** displayed the most significant antiproliferative effects, with an IC_{50} value of 6.4 ± 0.7 μM, thereby supporting the potential utility of mPGES-1 inhibition in controlling specific tumor phenotypes. However, under identical experimental conditions, treatment of healthy control cultures (HaCaT cell line) with both compounds resulted in moderate cytotoxicity, associated with IC_{50} values of approximately 17 and 28 μM for compounds **7d** and **7e**, respectively. Moreover, the analysis of biological effects in cultured cells reveals that, at lower concentrations, cellular responses directly correlated with the *in vitro* concentration of the tested compounds. As the concentration increases, concentration-effect curves tend to a plateau becoming almost independent of the concentration. Therefore, further efforts will be devoted to understand better and optimize the biological behavior of these compounds for preclinical development, aiming to enhance their safety profile and selectivity towards tumor cells.

3. Conclusions

This study highlights the potential of new furazanopyrazine-based compounds as promising anticancer agents through an interdisciplinary approach. Starting from the promising data obtained on hit compounds previously identified by us, we successfully identified and synthesized novel derivatives by replacing the functional ester group with a more stable ether moiety, thereby enhancing pharmacokinetic

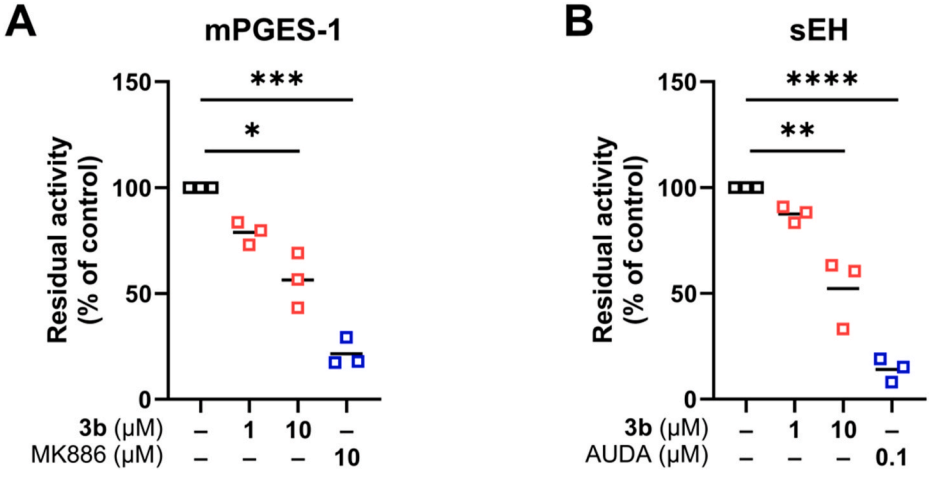

Fig. 8. Dual inhibition of mPGES-1 and sEH by **3b**. Data of individual measurements ($n = 3$) and the resulting mean are expressed as percentage relative to the vehicle-treated control. Statistical analysis was performed on raw data by RM one-way ANOVA and Dunnett's multiple comparisons test with single pooled variance. *$p < 0.05$; **$p < 0.01$; ***$p < 0.001$; ****$p < 0.0001$.

Table 2
Microsomal stability of test compounds in the presence of NADPH and UDPGA.

Structure	Compound	% parent compound depletion (h)100 - [concentration at time points min/concentration at 0 min] × 100				In vitro half-life (min)	Microsomal Intrinsic Clearance ($CL_{int,\ micr}$)(μL min^{-1} mg^{-1})	Calculated *in vivo* intrinsic (hepatic) Clearance (CL_{int}) (mL min^{-1} Kg^{-1})
		0.5	1.0	1.5	2.0	0.693/k, where k is the slope of linear regression of the percentage parent compound remaining against time	ln $2/t_{1/2}$ × [volume of incubation medium (μl)/ microsomal protein in incubation (mg)]	$CL_{int,\ micr}$ × (mg microsome g^{-1} liver) × [liver mass (g)/body mass (kg)]
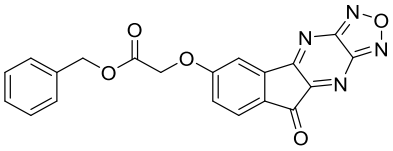	**3b**	99.9 ± 0.1	–	–	–	4.5	307.01	252.49
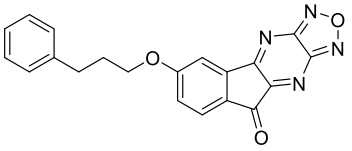	**7e**	5.0 ± 0.6	13.9 ± 1.3	20.4 ± 0.3	20.6 ± 0.2	325.9	4.25	3.50
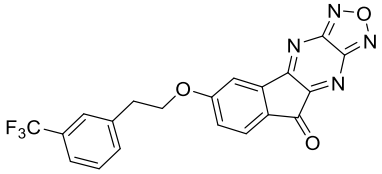	**7d**	11.2 ± 1.7	20.9 ± 0.2	36.4 ± 0.2	38.6 ± 2.2	158.8	8.73	7.18
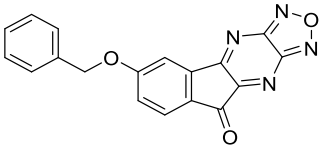	**7a**	6.2 ± 0.8	23.2 ± 0.3	30.1 ± 0.7	38.4 ± 0.1	164.6	8.42	6.92
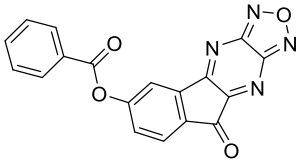	**BEO1**	26.1 ± 0.1	58.4 ± 0.2	63.9 ± 0.2	67.9 ± 0.2	69.6	19.93	16.39
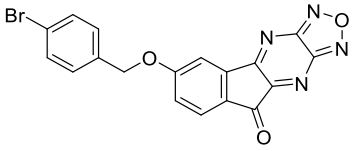	**7b**	4.2 ± 0.2	14.8 ± 1.6	26.7 ± 0.5	26.1 ± 0.2	238.2	5.82	4.78
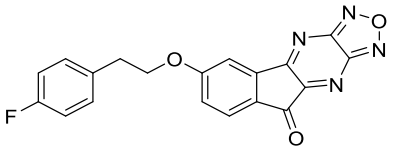	**7c**	36.7 ± 2.2	69.3 ± 0.9	78.8 ± 2.1	84.7 ± 0.7	42.9	32.32	26.58

properties while preserving anti-inflammatory activity. The building and screening of a focused virtual library led to the selection and synthesis of promising candidates, which demonstrated significant inhibitory activity against mPGES-1.

In order to further investigate the synthesized molecules, their ability to also interfere with soluble epoxide hydrolase (sEH) activity was studied *in silico* and with specific biological assays. The obtained results revealed the potential of compound **3b** to inhibit, together with mPGES-1, the soluble epoxide hydrolase (sEH) enzyme and to disclose furazanopyrazine-based compounds acting as dual-target inhibitors within the AA cascade, suggesting a cooperative inhibition mechanism. Unfortunately, compound **3b** did not reveal a promising pharmacokinetic profile among the set of screened compounds and, accordingly, we aim to exploit this structural information in the future to develop new derivatives that retain this promising multi-target inhibitory activity and feature an improved pharmacokinetic profile.

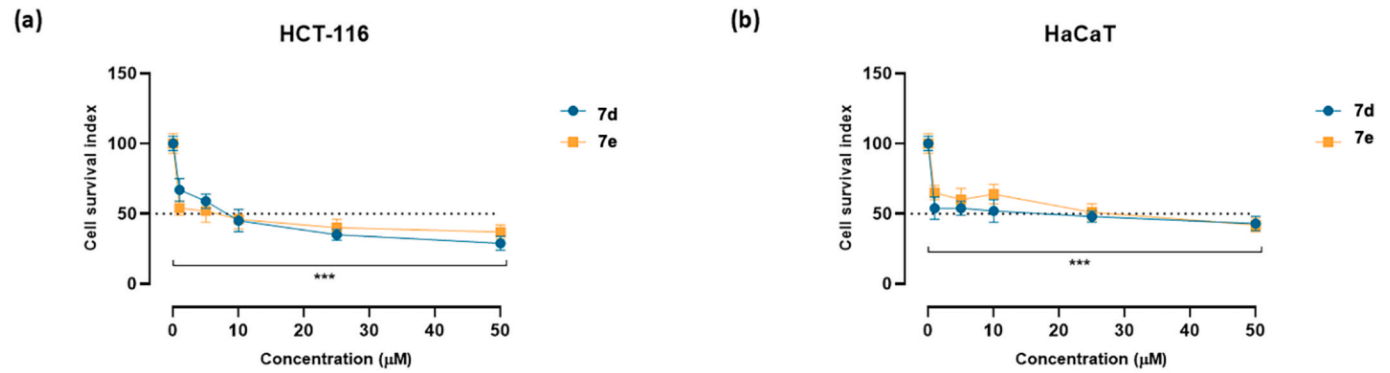

Fig. 9. Cell survival index, evaluated by the MTT assay and live/dead cell ratio, for (A) HCT-116 and (B) HaCaT cell lines following 48 h of incubation with the indicated concentrations (0–50 μM) of **7d** and **7e** as indicated in the legend. Data are expressed as a percentage of untreated control cells and are reported as the mean of four independent experiments ± SEM ($n = 24$). The cell survival index was calculated as described in the experimental section and plotted in line graphs against the different concentrations of the tested molecules. ***$p < 0.001$ vs. control cells.

Table 3
IC_{50} values (μM) relative to **7d** and **7e** in the indicated cancer cell line (HCT-116) and healthy cells (HaCaT) following 48 h of incubation. IC_{50} values are calculated from concentration-effect curves and reported as mean values ± SEM ($n = 24$).

	IC_{50} ± SEM (μM)	
Compound	HTC-116	HaCat
7d	8.3 ± 1.1	17 ± 2.0
7e	6.4 ± 0.7	28 ± 1.5

Given the involvement of mPGES-1 in human CRC, compounds that emerged as most active against mPGES-1 and, simultaneously, showed a promising pharmacokinetic profile, confirmed by studies conducted on human liver microsomes (**7d** and **7e**), were tested on the HCT-116 cell line, revealing moderate antiproliferative effects that highlight their potential as novel putative therapeutic agents.

Overall, the combination of computational design, chemical synthesis, and biological evaluation led to the successful identification of furazanopyrazine derivatives as a novel class of anti-inflammatory and anticancer drugs. The encouraging results of this study pave the way for further development and optimization of these compounds, potentially leading to novel therapeutic alternatives for treating chronic inflammatory diseases and associated illnesses, including cancer.

4. Experimental section

4.1. Computational detail

4.1.1. Building of a combinatorial library and virtual screening

Interactive Enumeration tool of CombiGlide software was employed to build two virtual libraries of 5848 furazanopyrazine-based compounds: according to the synthetic scheme, 5848 commercially available alkyl halides, containing at least an aromatic ring, (downloaded from Sigma-Aldrich and prepared by Reagent Preparation) were used to generate the library [38]. Subsequently, pharmacokinetic properties were calculated by QikProp software (Schrödinger Suite) for all generated compounds [39]. The application of pharmacokinetic filters based on Lipinski's rule of five allowed compounds with an unfavorable ADME profile to be discarded. Then, the remaining 5237 molecules of each library were subjected to molecular docking-virtual screening campaigns.

Compounds **3a**, **7a**, **8a**, **12**, and **13** were drawn by 2D Sketcher of Maestro (Schrödinger Suite) and prepared using LigPrep software (Schrödinger Suite) [40] at a pH = 7.4 ± 1.0, and the structures obtained were minimized using OPLS 2005 force field.

4.1.2. Virtual Screening Workflow on mPGES-1

The X-ray crystal of mPGES-1 co-crystallized with the inhibitor LVJ (PDB ID: 4BPM [18]) was downloaded by RCS PDB and prepared using Protein Preparation Wizard (Schrödinger Suite) [41,42]: cap termini were incorporated, hydrogen atoms were introduced, and bond orders were assigned after the removal of all water molecules, solvent, and co-complexed compound. The centroid of the active site was defined by accounting for the grid box in molecular docking experiments using the co-crystallized ligand as a guide. The final coordinates of the grid center were 22.63 (x), 48.39 (y), 78.66 (z) and the inner and outer box dimensions were of 10 × 10 × 10 and 26.66 × 26.66 × 26.66, respectively.

The Virtual Screening was performed using the Virtual Screening Workflow tool as implemented in Schrödinger Suite, considering three levels of precision:

- High-Throughput Virtual Screening (HTVS) scoring and sampling phase: saved first 80 % of compounds ranked by docking score;
- Standard Precision (SP) scoring and sampling phase: saved first 80 % ranked compounds;
- Extra Precision (XP) scoring and sampling generated 10 poses for each ligand. Compounds ranked in the top 90 % based on the docking score were selected and constituted the final output.

Compounds were visually examined and selected based on their adherence to the critical interactions for the subsequent chemical synthesis phase.

4.1.3. Molecular docking experiments on soluble epoxide hydrolase (sEH)

The X-ray crystal structure of sEH in complex with the inhibitor BSU (1,3-diphenylurea) (PDB ID: 5AI5 [26]) was retrieved by Protein Data Bank and prepared using Protein Preparation Wizard (Schrödinger Suite) [41,42]: all water molecules, solvent and co-complexed compound were removed, cap termini were incorporated, hydrogen atoms were added, and bond orders were assigned. The grid box for molecular docking experiments was determined using the co-crystallized ligand to define the centroid of the active site. The final coordinates of the grid center were −16.43 (x), −11.02 (y), 15.93 (z) and the inner and outer box dimensions were of 10 × 10 × 10 and 23.94 × 23.94 × 23.94, respectively. Molecular docking experiments were performed using Glide software and the Extra Precision (XP) mode [43–47]. Specifically, during the initial docking phase, 10000 poses were kept and evaluated to select 800 conformations, which were subjected to the minimization step with an energy threshold of 0.15 kcal/mol. Finally, a maximum of 20 poses were retained for subsequent analysis to examine the binding mode.

4.2. General synthetic procedures

Materials. Inorganics, organic reagents, and solvents were commercial pure compounds and used without further purification. TLC analyses were performed using silica gel plates (silica gel 60 F-254) visualized by UV light, fluorescent light, and iodine.

Column chromatographies were carried out on silica gel (70–230 mesh). ^{1}H and ^{13}C NMR spectra were recorded on Varian Inova 500 MHz and BrukerAvance 400 MHz spectrometers: chemical shifts in ppm (δ) and J coupling constants in Hz. All ^{13}C NMR spectrum are proton/fluorine decoupled. The following abbreviations are used to indicate the multiplicity: s, singlet; d, doublet; m, multiplet; b, broad signal. Elemental analysis was performed in duplicate using a Flash Smart V CHNS instrument (Thermo Fischer). Melting points were determined on a Fischer Scientific melting point apparatus. Abbreviations, NBS: *N*-bromosuccinimide; DMF: *N*,*N*-dimetilformammide; DMSO: dimethylsulfoxide; PLC: Preparative Layer Plates.

4.2.1. Synthesis of 9-oxo-9H-2-oxa-1,3,4,10-tetraazacyclopenta[b]fluoren-6-yl cyclohexanecarboxylate (3a)

In 100 mL round bottom flask charged with a magnetic stirrer, cyclohexanecarbonyl chloride (1.47 g, 10.0 mmol) was added to compound **2** (3.60 g, 15.0 mmol) and K_2CO_3 (2.07 g, 15.0 mmol) in 20 mL of DMF. The resulting mixture was stirred for 24 h at room temperature. The reaction was quenched with 50 mL H_2O and the aqueous phase was extracted with diethyl ether (3 × 40 mL). The organic phase was washed with 2 N NaOH (2 × 20 mL), dried over Na_2SO_4 and concentrated under reduced pressure. The residue was purified by flash column chromatography on silica gel (hexane:ethyl acetate, 7:3) to give the compound **3a** as Yellow solid. Yield 20.0 %. M.p. = 116 °C. **^{1}H NMR** (500 MHz, DMSO-d_6): δ 8.33 (d, J = 8.1 Hz, 1H), 8.28 (bs, 1H), 7.87 (d, J = 8.1 Hz, 1H), 2.88 (m, 1H), 2.20 (m, 2H), 1.92 (m, 2H), 1.80 (m, 1H), 1.71 (m, 2H), 1.37–1.61 (m, 3H). **^{13}C NMR** (125 MHz, DMSO-d_6): δ 184.3, 173.7, 161.4, 158.0, 153.8, 153.6, 153.5, 141.6, 138.0, 129.9, 127.2, 118.2, 42.6, 28.7, 25.7, 25.1. Anal. Calcd. for $C_{18}H_{14}N_4O_4$: C, 61.71 %; H, 4.030 %; N, 15.99 %; found: C, 61.56 %; H, 4.160 %; N, 15.81 %. HRMS (ESI) calcd. [M+H]+ 351.1015, found 351.1021.

Under the same conditions the following compounds were prepared.

4.2.2. Benzyl 2-((9-Oxo-9H-2-oxa-1,3,4,10-tetraazacyclopenta[b]fluoren-6-yl)oxy)acetate (3b)

Prepared in 20.0 % yield using benzyl bromoacetate. Yellow solid. M.p. = 186 °C. **^{1}H NMR** (500 MHz, $CDCl_3$): δ 8.05 (d, J = 8.6 Hz, 1H), 7.58 (d, J = 2.3 Hz, 1H), 7.41–7.34 (m, 6H), 5.29 (s, 2H), 4.94 (s, 2H). **^{13}C NMR** (125 MHz, $CDCl_3$): δ 182.4, 166.9, 165.7, 161.4, 159.5, 152.8, 142.4, 142.3, 135.0, 134.6, 128.9, 128.8, 128.7, 127.8, 124.4, 107.4, 67.7, 65.6. Anal. Calcd. for $C_{20}H_{12}N_4O_5$: C, 61.86 %; H, 3.110 %; N, 14.43 %; found: C, 61.75 %; H, 3.010 %; N, 14.53 %. HRMS (ESI) calcd. $[M+H]^+$ 389.0808, found 389.0878.

4.2.3. 6-(3-(Benzyloxy)propoxy)-2-oxa-1,3,4,10-tetraazacyclopenta[b]fluoren-9-one (3c)

Prepared in 25.0 % yield using benzyl-3-bromopropyl ether. Brown Mustard solid. M.p. = 199–200 °C. **^{1}H NMR** (500 MHz, $CDCl_3$): 8.04 (d, J = 8.6 Hz, 1H), 7.67 (d, J = 2.3 Hz, 1H), 7.44 (dd, J = 8.4 and 2.3 Hz, 1H), 7.28–7.35 (m, 5H), 4.55 (bs, 2H), 4.38 (t, J = 6.3 Hz, 2H), 3.69 (dd, J = 10.8 and 5.8 Hz, 2H), 2.19 (m, 2H); **^{13}C NMR** (125 MHz, $CDCl_3$): δ 186.5, 162.6, 153.9, 149.9, 148.9, 143.2, 140.1, 137.9, 129.5, 128.4, 127.6, 127.6, 127.3, 114.9, 109.4, 73.1, 66.3, 66.0, 29.6. Anal. Calcd. for $C_{21}H_{16}N_4O_4$: C, 64.94 %; H, 4.150 %; N, 14.43 %. Found: C, 65.13 %; H, 4.050 %; N, 14.54 %. HRMS (ESI) calcd. $[M+H]^+$ 389.1172, found 389.1240.

4.2.4. Synthesis of 2,3-dihydro-5-(phenylmethoxy)-1H-inden-1-one (5a)

To 5-hydroxy-1-indanone (0.222 g, 1.50 mmol) and K_2CO_3 (0.207 g, 1.50 mmol) dissolved in 2.0 mL of DMF, benzyl bromide (0.171 g, 1.00 mmol) was added. The reaction mixture was stirred for 24 h at room temperature, then was quenched with 50 mL H_2O and the aqueous phases were extracted with diethyl ether (3 x 40 mL). The organic phase was washed with 2 N NaOH (2 x 20 mL) to remove the excess of phenol, dried over Na_2SO_4 and concentrated under reduced pressure. The residue was purified by flash column chromatography on silica gel (hexane: ethyl acetate, 9:1) to give the compound **5a** as Yellowish solid. Yield 60.0 %. M.p. = 107 °C. **^{1}H NMR** (500 MHz, DMSO-d_6): δ 7.56 (d, J = 8.5 Hz, 1H), 7.47 (m, 2H), 7.41 (t, J = 7.3 Hz, 2H), 7.35 (m, 1H), 7.19 (bs, 1H), 7.03 (dd, J = 8.5 and 2.0 Hz, 1H), 5.23 (s, 2H), 3.05 (m, 2H), 2.59 (m, 2H). **^{13}C NMR** (125 MHz, DMSO-d_6): δ 204.7, 164.3, 158.7, 136.9, 130.5, 129.0, 128.5, 128.3, 125.1, 116.3, 111.6, 70.2, 36.5, 25.9. Anal. Calcd. for $C_{16}H_{14}O_2$: C, 80.65 %; H, 5.920 %; found: C, 80.51 %; H, 6.050 %.

Under the same conditions the following compounds were prepared.

4.2.5. 5-[(4-Bromophenyl)methoxy]-2,3-dihydro-1H-inden-1-one (5b)

Prepared in 90.0 % yield using 4-bromobenzyl bromide. Yellow Solid. M.p. = 128–129 °C. **^{1}H NMR** (500 MHz, $CDCl_3$): δ 7.71 (d, J = 8.2 Hz, 1H), 7.54 (d, J = 8.1 Hz, 2H), 7.32 (d, J = 8.1 Hz, 2H), 6.94–7.00 (m, 2H), 5.11 (s, 2H), 3.10 (m, 2H), 2.69 (m, 2H). **^{13}C NMR** (125 MHz, $CDCl_3$): δ 205.2, 164.0, 158.1, 135.1, 131,9, 130.8, 129.0, 125.5, 122.2, 115.8, 110.8, 69.5, 36.4, 25.9. Anal. Calcd. for $C_{16}H_{13}BrO_2$: C, 60.59 %; H, 4.130 %; found: C, 60.79 %; H, 4.020 %.

4.2.6. 5-[2-(4-Fluorophenyl)ethoxy]-2,3-dihydro-1H-inden-1-one (5c)

Prepared in 42.0 % yield using 4-fluorophenethyl bromide. Yellow-green solid. M.p. = 177 °C. **^{1}H NMR** (500 MHz, $CDCl_3$): δ 7.67 (d, J = 9.2 Hz, 1H), 7.24 (m, 2H), 7.00 (m, 2H), 6.86–6.91 (m, 2H), 4.22 (t, J = 6.8 Hz, 2H), 3.03–3.13 (m, 4H), 2.66 (m, 2H); **^{13}C NMR** (125 MHz, $CDCl_3$): δ 205.1, 171.0, 164.2, 162.8, 160.4, 157.9, 130.2, 125.3, 115.4, 115.1, 110.2, 68.8, 36.2, 34.0, 25.7. Anal. Calcd. for $C_{17}H_{15}FO_2$: C, 75.54 %; H, 5.590 %; found: C, 75.64 %; H, 5.450 %.

4.2.7. 5-[3-(Trifluoromethyl)phenethoxy]-2,3-dihydro-1H-inden-1-one (5d)

Prepared in 36.0 % yield using 3-(trifluoromethyl)phenethyl bromide. Yellow solid. M.p. = 171 °C. **^{1}H NMR** (400 MHz, $CDCl_3$): δ 7.67 (d, J = 9.1 Hz, 1H), 7.55 (bs, 1H), 7.41–7.53 (m, 3H), 6.86–6.91 (m, 2H), 4.26 (t, J = 6.6 Hz, 2H), 3.18 (t, J = 6.6 Hz, 2H), 3.06 (m, 2H), 2.65 (m, 2H); **^{13}C NMR** (100 MHz, $CDCl_3$): δ 205.1, 164.1, 158.0, 138.7, 132.2, 130.4, 128.8, 125.6, 125.2, 123.5, 123.4, 123.4, 115.4, 110.2, 68.3, 36.2, 35.2, 25.7. Anal. Calcd. for $C_{18}H_{15}F_3O_2$: C, 67.50 %; H, 4.720 %; found: C, 67.51 %; H, 4.770 %.

4.2.8. 5-(3-Phenylpropoxy)-2,3-dihydro-1H-inden-1-one (5e)

Prepared in 70.0 % yield using 1-bromo-3-phenylpropane. Light yellow solid. M.p. = 74 °C. **^{1}H NMR** (400 MHz, $CDCl_3$): δ 7.70 (d, J = 8.4 Hz, 1H), 7.29–7.35 (m, 2H), 7.21–7.26 (m, 3H), 6.92 (dd, J = 8.5, 2.1 Hz, 1H), 6.89 (bs, 1H), 4.05 (t, J = 6.3 Hz, 2H), 3.10 (m, 2H), 2.85 (m, 2H), 2.69 (m, 2H), 2.17 (m, 2H); **^{13}C NMR** (100 MHz, $CDCl_3$): δ 205.1, 164.5, 158.0, 141.0, 130.2, 128.3, 128.3, 125.9, 125.2, 115.5, 110.1, 67.1, 36.3, 31.9, 30.4, 25.7. Anal. Calcd. for $C_{18}H_{18}O_2$: C, 81.17 %; H, 6.810 %; found: C, 81.02 %; H, 6.950 %.

4.2.9. Synthesis of 2,2-dihydroxy-1,3-dioxo-indan-4-yl derivates (6a-e)

4.2.9.1. Classical procedure. *N*-bromosuccinimide (0.671 g, 3.60 mmol) was added to protected phenol (**5a-e**) (1.80 mmol) in 9.0 mL of dimethylsulfoxide. The reaction mixture was stirred at 60 °C for 3 h and then at 80 °C for 4 h. Finally, the reaction was cooled to room temperature and poured into 200 mL of water. The product was extracted with three portions of 100 mL of CH_2Cl_2, and then the combined organic extracts were dried (sodium sulfate), filtered and evaporated. The residue was used without any further purification for the next step of reaction.

4.2.9.2. Microwave procedure. In a 10 mL Pyrex microwave vial, Selenium dioxide (0.344 g, 3.10 mmol) was added to a solution-protected phenol (**5a-e**) (1.00 mmol) in dioxane:H_2O 10 % (v/v). The reaction vial was sealed with a snap-on cap and was shook until a dark solution was obtained. The mixture was subjected to microwave heating for 5 min (hold time) at 180 °C (internal probe, power 300 W). The overall crude was filtered on Whatman paper and was washed with Acetone. The residue was used without any further purification for the next step of the reaction.

*4.2.10. Synthesis of 6- and 7-phenylmethoxy-2-oxa-1,3,4,10-tetraazacyclopenta[b]fluoren-9-one (**7a** and **8a**)*

4.2.10.1. Classical procedure. A mixture of **6a** (0.142 g, 0.500 mmol) and furazan-3,4-diamine (0.050 g, 0.500 mmol) in 1.5 mL of ethanol and 1.5 mL of glacial acetic acid was stirred at room temperature for 18 h and then heated at reflux for 6 h. The solid was filtered and washed with water, and the residue was purified by silica gel chromatography (hexane:ethyl acetaye, 7:3) to give the regioisomers **7a** and **8a** in ratio 1:0.88, respectively.

*4.2.11. 6-Phenylmethoxy-2-oxa-1,3,4,10-tetraazacyclopenta[b]fluoren-9-one (**7a**)*

Yield 26.6 %. Yellow solid. M.p. = 186 °C. **^{1}H NMR** (500 MHz, DMSO-d_6): δ 8.06 (d, J = 8.1 Hz, 1H), 7.85 (bs, 1H), 7.56 (m, 1H), 7.53 (d, J = 8.0 Hz, 2H), 7.44 (m, 2H), 7.38 (m, 1H), 5.49 (s, 2H); **^{13}C NMR** (125 MHz, DMSO-d_6): δ 183.8, 166.4, 163.5, 162.1, 154.0, 153.6, 142.9, 136.2, 134.7, 129.1, 128.8, 128.4, 127.6, 124.7, 108.2, 71.0. Anal. Calcd. for $C_{18}H_{10}N_4O_3$: C, 65.45 %; H, 3.050 %; N, 16.96 %; found: C, 65.55 %; H, 3.070 %; N, 16.89 %. HRMS (ESI) calcd. $[M+H]^+$ 331.0753, found 331.0820.

*4.2.12. 7-Phenylmethoxy-2-oxa-1,3,4,10-tetraazacyclopenta[b]fluoren-9-one (**8a**)*

Yield 23.4 %. Yellow solid. M.p. = 183 °C. **^{1}H NMR** (500 MHz, DMSO-d_6): δ 8.25 (d, J = 7.5 Hz, 1H), 7.66 (m, 2H), 7.53 (d, J = 7.4 Hz, 2H), 7.44 (m, 2H), 7.38 (m, 1H), 5.44 (s, 2H); **^{13}C NMR** (125 MHz, DMSO-d_6): δ 185.3, 164.8, 164.5, 163.2, 162.1, 153.6, 143.0, 136.3, 133.2, 129.1, 128.7, 128.4, 126.9, 126.5, 109.0, 70.9. Anal. Calcd. for $C_{18}H_{10}N_4O_3$: C, 65.45 %; H, 3.050 %; N, 16.96 %; found: C, 65.43 %; H, 3.090 %; N, 16.95 %. HRMS (ESI) calcd. $[M+H]^+$ 331.0753, found 331.0821.

Under the same conditions the following compounds were prepared.

*4.2.13. 6-[(4-Bromophenyl)methoxy]-2-oxa-1,3,4,10-tetraazacyclopenta[b]fluoren-9-one (**7b**)*

Yield 35.0 %. Yellow solid. M.p. = 198 °C. **^{1}H NMR** (500 MHz, DMSO-d_6): δ 8.07 (d, J = 8.5 Hz, 1H), 7.84 (d, J = 2.1 Hz, 1H), 7.64 (d, J = 8.6 Hz, 2H), 7.53–7.46 (m, 3H), 5.48 (s, 2H); **^{13}C NMR** (125 MHz, $CDCl_3$): δ 187.3, 166.4, 161.4, 158.1, 154.7, 147.3, 143.8, 140.1, 136.7, 134.6, 129.3, 127.9, 125.9, 112.3, 108.4, 70.4. Anal. Calcd. for $C_{18}H_9BrN_4O_3$: C, 52.83 %; H, 2.22 %; N, 13.69 %; found: C, 52.82 %; H, 2.410 %; N, 13.55 %. HRMS (ESI) calcd. $[M+H]^+$ 408.9858, found 408.9865.

*4.2.14. 7-[(4-Bromophenyl)methoxy]-2-oxa-1,3,4,10-tetraazacyclopenta[b]fluoren-9-one (**8b**)*

Yield 24.0 %. Yellow ocher solid. M.p. = 205–206 °C. **^{1}H NMR** (500 MHz, DMSO-d_6): δ 8.24 (d, J = 8.8 Hz, 1H), 7.71–7.59 (m, 3H), 7.53–7.45 (m, 3H), 5.42 (s, 2H); **^{13}C NMR** (125 MHz, DMSO-d_6): δ 188.2, 166.8, 162.7, 159.6, 154.0, 147.8, 146.1, 140.2, 135.7, 132.0, 130.5, 127.7, 124.6, 121.9, 108.2, 70.3. Anal. Calcd. for $C_{18}H_9BrN_4O_3$: C, 52.83 %; H, 2.220 %; N, 13.69 %; found: C, 52.75 %; H, 2.110 %; N, 13.78 %. HRMS (ESI) calcd. $[M+H]^+$ 408.9858, found 408.9865.

*4.2.15. 6-[2-(4-Fluorophenyl)ethoxy]-2-oxa-1,3,4,10-tetraazacyclopenta[b]fluoren-9-one (**7c**)*

Yield 35.1 %. Light yellow-green solid. M.p. = 201–204 °C. **^{1}H NMR** (500 MHz, $CDCl_3$): δ 8.05 (d, J = 8.6 Hz, 1H), 7.67 (bs, 1H), 7.34 (d, J = 8.6 Hz, 1H), 7.32–7.28 (m, 2H), 7.07 (t, J = 8.3 Hz, 2H), 4.45 (t, J = 6.6 Hz, 2H), 3.21 (t, J = 6.6 Hz, 2H). **^{13}C NMR** (125 MHz, DMSO-d_6): δ 186.4, 166.6, 162.5, 160.4, 153.7, 148.0, 142.9, 134.5, 131.3, 129.0, 127.7, 124.3, 115.6, 115.5, 108.0, 70.1, 34.1. Anal. Calcd. for $C_{19}H_{11}FN_4O_3$: C, 62.99 %; H, 3.060 %; N, 15.46 %, found: C, 63.16 %; H, 3.010 %; N, 15.39 %. HRMS (ESI) calcd. $[M+H]^+$ 363.0815, found 363.0883.

*4.2.16. 7-[2-(4-Fluorophenyl)ethoxy]-2-oxa-1,3,4,10-tetraazacyclopenta[b]fluoren-9-one (**8c**)*

Yield 25.0 %. Light yellow-green solid. M.p. = 200–203 °C. **^{1}H NMR** (500 MHz, $CDCl_3$): δ 8.22 (d, J = 8.1 Hz, 1H), 7.50–7.45 (m, 3H), 7.30 (m, 1H), 7.06 (m, 2H), 4.39 (t, J = 6.5 Hz, 2H), 3.19 (t, J = 6.5 Hz, 2H); **^{13}C NMR** (125 MHz, $CDCl_3$): δ 184.6, 167.5, 160.0, 152.9, 149.4, 144.9, 141.0, 136.9, 132.8, 130.4, 130.0, 127.8, 122.6, 115.6, 108.1, 70.2, 34.6. Anal. Calcd. for $C_{19}H_{11}FN_4O_3$: C, 62.99 %; H, 3.060 %; N, 15.46 %; found: C, 62.91 %; H, 3.020 %; N, 15.49 %. HRMS (ESI) calcd. $[M+H]^+$ 363.0815, found 363.0883.

*4.2.17. 6-[3-(Trifluoromethyl)phenethoxy]-2-oxa-1,3,4,10-tetraazacyclopenta[b]fluoren-9-one (**7d**)*

Yield 25.0 %. Yellow-green solid. M.p. = 235–236 °C. **^{1}H NMR** (500 MHz, DMSO-d_6): δ 8.03 (d, J = 8.5 Hz, 1H), 7.80 (d, J = 1.4 Hz, 1H), 7.76 (m, 1H), 7.71 (d, J = 7.1 Hz, 1H), 7.64–7.54 (m, 2H), 7.46 (m, 1H), 4.62 (t, J = 6.6 Hz, 2H), 3.26 (t, J = 6.6 Hz, 2H); **^{13}C NMR** (125 MHz, DMSO-d_6): δ 183.6, 166.5, 162.1, 154.0, 153.7, 142.9, 142.9, 139.8, 134.7, 134.7, 133.8, 129.8, 128.8, 127.7, 126.1, 124.3, 123.7, 108.0, 69.7, 34.6. Anal. Calcd. for $C_{20}H_{11}N_4O_3F_3$: C, 58.26 %; H, 2.690 %; N, 13.59 %; found: C, 58.43 %; H, 2.790 %; N, 13.49 %. HRMS (ESI) calcd. [M+H]+ 413.0783, found 413.0850.

*4.2.18. 7-[3-(Trifluoromethyl)phenethoxy]-2-oxa-1,3,4,10-tetraazacyclopenta[b]fluoren-9-one (**8d**)*

Yield 18.0 %. Yellow-green solid. M.p. = 231–233 °C. **^{1}H NMR** (500 MHz, DMSO-d_6): δ 8.22 (bs, 1H), 7.83–7.75 (m, 2H), 7.70 (d, J = 6.6 Hz, 1H), 7.65–7.55 (m, 3H), 4.57 (t, J = 6.5 Hz, 2H), 3.25 (t, J = 6.5 Hz, 2H); **^{13}C NMR** (125 MHz, DMSO-d_6): δ 186.5, 166.5, 162.1, 153.7, 143.0, 141.6, 139.9, 136.9, 133.7, 133.2, 129.8, 126.8, 126.5, 126.1, 124.3, 123.7, 123.2, 108.8, 69.5, 34.6. Anal. Calcd. for $C_{20}H_{11}F_3N_4O_3$: C, 58.26 %; H, 2.690 %; N, 13.59 %; found: C, 58.22 %; H, 2.700 %; N, 13.45 %. HRMS (ESI) calcd. $[M+H]^+$ 413.0783, found 413.0849.

*4.2.19. 6-[3-Phenylpropoxy]-2-oxa-1,3,4,10-tetraazacyclopenta[b]fluoren-9-one (**7e**)*

Yield 36.0 %. Brown Mustard solid. M.p. = 196 °C. **^{1}H NMR** (500 MHz, DMSO-d_6): δ 8.05 (bs, 1H), 7.75 (bs, 1H), 7.49 (bs, 1H), 7.17–7.35 (m, 5H), 4.33 (bs, 2H), 2.82 (t, J = 7.4 Hz, 2H), 2.13 (m, 2H); **^{13}C NMR** (125 MHz, DMSO-d_6): δ 183.8, 167.1, 154.4, 149.8, 148.9, 143.1, 142.0, 137.6, 134.7, 128.7, 128.8, 127.8, 126.4, 124.3, 107.9, 69.2, 31.7, 30.4. Anal. Calcd. for $C_{20}H_{14}N_4O_3$: C, 67.03 %; H, 3.940 %; N, 15.63 %; found: C, 67.21 %; H, 3.990 %; N, 15.49 %. HRMS (ESI) calcd. $[M+H]^+$ 359.1066, found 359.1133.

*4.2.20. 7-[3-phenylpropoxy]-2-oxa-1,3,4,10-tetraazacyclopenta[b]fluoren-9-one (**8e**)*

Yield 21.0 %. Brown Mustard solid. M.p. = 191 °C. **^{1}H NMR** (500 MHz, $CDCl_3$): δ 8.22 (d, J = 8.4 Hz, 1H), 7.51–7.45 (m, 2H), 7.35 (s, 1H), 7.33 (d, J = 7.4 Hz, 2H), 7.24 (d, J = 7.4 Hz, 2H), 4.19 (t, J = 6.5 Hz, 2H), 2.88 (t, J = 7.5 Hz, 2H), 2.24 (m, 2H); **^{13}C NMR** (125 MHz, $CDCl_3$): δ 187.3, 165.8, 158.3, 150.9, 148.6, 144.9, 140.6, 137.5, 134.8, 128.6, 128.2, 126.6, 125.0, 122.3, 108.2, 64.5, 33.5, 29.7. Anal. Calcd. for $C_{20}H_{14}N_4O_3$: C, 67.03 %; H, 3.940 %; N, 15.63 %. Found: C, 67.01 %; H,

3.950 %; N, 15.71 %. HRMS (ESI) calcd. $[M+H]^+$ 359.1066, found 359.1134.

4.2.20.1. Microwave procedure. In a 10 mL Pyrex microwave vial, furazan-3,4-diamine (50 mg, 0.5 mmol) was added to a solution of **6a** (0.142 g, 0.500 mmol) in EtOH:AcOH (1:1) (v/v). The reaction vial was sealed with a snap-on cap and was shook until a dark solution was obtained. The mixture was subjected to microwave heating for 5 min (hold time) at 180 °C (internal probe, power 300 W). The overall crude was filtered on Whatman paper and was purified by PLC (CH_2Cl_2). (Yields are reported in Table 1 of the manuscript).

*4.2.21. Synthesis of N-(2,3-dihydro-1-oxo-1H-inden-5-yl)benzamide (**10**)*

5-Amino-2,3-dihydro-1*H*-inden-1-one (**9**) (0.147 g, 1.00 mmol) was dissolved in 3.0 ml of 10 % aqueous sodium hydroxide solution in a 25 mL flask. Solutions of tetra-*n*-butylammonium chloride (0.028 g, 0.10 mmol) in 1.0 mL of CH_2Cl_2 and benzoyl chloride (0.281 g, 0.232 mL, 2.00 mmol) in 1.0 mL of CH_2Cl_2 were prepared. After cooling all solutions at 0 °C, they were mixed at once. The reaction mixture was kept under vigorous magnetic stirring at reflux for 24 h. After the removal of the solvent under reduced pressure, the residue was diluted with brine and extracted with CH_2Cl_2. After drying on Na_2SO_4, the solvent was evaporated and the residue was purified by silica gel chromatography (hexane:ethyl acetate, 7:3) to give the compound **10** as light brown solid. Yield 70.0 %. M.p. = 74–75 °C. **^{1}H NMR** (500 MHz, $CDCl_3$): δ 8.19 (d, J = 8.2 Hz, 1H), 8.06 (bs, 1H, NH), 7.93 (d, J = 8.2 Hz, 1H), 7.83 (d, J = 1.6 Hz, 1H), 7.49–7.63 (m, 5H), 3.17 (m, 2H), 2.76 (m, 2H); **^{13}C NMR** (125 MHz, $CDCl_3$): δ 206.5, 168.1, 151.0, 140.7, 137.7, 137.6, 132.1, 128.9, 127.3, 127.1, 119.9, 114.5, 36.7, 25.5. Calculated for $C_{16}H_{13}NO_2$: C, 76.48 %; H, 5.210 %; N, 5.570 %; found: C, 76.51 %; H, 5.330 %; N, 5.460 %.

*4.2.22. Synthesis of N-(2,2-dihydroxy-1,3-dioxo-indan-5-yl)benzamide (**11**)*

4.2.22.1. Classical procedure. N-bromosuccinimide (0.356 g, 2.00 mmol) was added to a solution of **10** (0.251 g, 1.00 mmol) in 5.0 mL of DMSO. The reaction mixture was stirred at 60 °C for 3 h and then at 80 °C for 4 h with a vacuum line attached to the top of the reaction flask condenser. The reaction mixture was cooled to room temperature and then poured into 200 mL of water. The product was extracted with three portions of 100 mL of CH_2Cl_2, and then the combined organic extracts were dried (sodium sulfate), filtered and evaporated. The residue was used without any further purification for the next step of the reaction.

4.2.22.2. Microwave procedure. In a 10 mL Pyrex microwave vial, Selenium dioxide (0.344 mg, 3.10 mmol) was added to a solution of **10** (0.251 g,1.00 mmol) in dioxane:H_2O 10 % (v/v). The reaction vial was sealed with a snap-on cap and was shook until a dark solution was obtained. The mixture was subjected to microwave heating for 5 min (hold time) at 180 °C (internal probe, power 300 W). The overall crude was filtered on Whatman paper and was washed with acetone. The residue was used without any further purification for the next step of the reaction.

*4.2.23. Synthesis of N-(9-oxo-9H-2-oxa-1,3,4,10-tetraazacyclopenta[b] fluoren-6-yl)benzamide (**12**) and N-(9-oxo-9H-2-oxa-1,3,4,10-tetraazacyclopenta[b]fluoren-7-yl)benzamide (**13**)*

4.2.23.1. Classical procedure. A mixture of **11** (0.149 g, 0.500 mmol) and furazan-3,4-diamine (0.050 g, 0.50 mmol) in 1.5 mL of ethanol and 1.5 mL of glacial acetic acid was stirred at room temperature for 18 h and then heated at reflux for 6 h. The precipitated solid was filtered and washed with water and the residue was purified by silica gel chromatography (hexane:ethyl acetate, 7:3) to give the regioisomers **12** and **13** in ratio 1:0.88, respectively.

*4.2.24. N-(9-oxo-9H-2-oxa-1,3,4,10-tetraazacyclopenta[b]fluoren-6-yl) benzamide (**12**)*

Yield 13.3 %. Yellow ocher solid. M.p. = 293–296 °C. **^{1}H NMR** (500 MHz, DMSO-d_6): δ 11.11 (s, 1H, NH), 8.79 (bs, 1H), 8.26 (d, J = 8.4 Hz, 1H), 8.12 (d, J = 8.4 Hz, 1H), 8.02 (d, J = 7.2 Hz, 2H), 7.67 (m, 1H), 7.60 (d, J = 7.6 Hz, 2H); **^{13}C NMR** (125 MHz, DMSO-d_6): δ 183.9, 167.2, 163.6, 162.0, 153.6, 148.2, 141.7, 141.4, 136.1, 134.3, 133.0, 129.3, 129.1, 128.4, 126.9, 113.5. Anal. Calcd. for $C_{18}H_9N_5O_3$: C, 62.98 %; H, 2.640 %; N, 20.40 %; found: C, 62.87 %; H, 2.750 %; N, 20.35 %. HRMS (ESI) calcd. $[M+H]^+$ 344.0705, found 344.0771.

*4.2.25. N-(9-oxo-9H-2-oxa-1,3,4,10-tetraazacyclopenta[b]fluoren-7-yl) benzamide (**13**)*

Yield 11.7 %. Yellow ocher solid. M.p. = 286–286 °C. **^{1}H NMR** (500 MHz, DMSO-d_6): δ 11.02 (s, 1H, NH), 8.56 (bs, 1H), 8.37–8.38 (m, 2H), 8.02 (d, J = 7.2 Hz, 2H), 7.66 (m, 1H), 7.57 (d, J = 7.2 Hz, 2H); **^{13}C NMR** (125 MHz, DMSO-d_6): δ 185.5, 167.1, 163.1, 154.0, 153.7, 146.5, 141.4, 134.7, 134.4, 132.9, 129.3, 129.1, 128.5, 126.1, 126.1, 114.5. Anal. Calcd. for $C_{18}H_9N_5O_3$: C, 62.98 %; H, 2.640 %; N, 20.40 %; found: C, 62.99 %; H, 2.690 %; N, 20.32 %. HRMS (ESI) calcd. $[M+H]^+$ 344.0705, found 344.0770.

4.2.25.1. Microwave procedure. In a 10 mL Pyrex microwave vial, furazan-3,4-diamine (0.050 g, 0.50 mmol) was added to a solution of **11** (0.149 g, 0.500 mmol) in EtOH:AcOH (1:1) (v/v). The reaction vial was sealed with a snap-on cap and was shook until a dark solution was obtained. The mixture was subjected to microwave heating for 5 min (hold time) at 180 °C (internal probe, power 300 W). The overall crude was filtered on Whatman paper and was washed with acetone. The residue was purified by PLC (CH_2Cl_2) to yield 27 % of regioisomers **12** and **13** in ratio 1:0.78 respectively.

4.3. In vitro drug metabolism studies using human liver microsomes

4.3.1. Instrumentation and analytical conditions

The metabolic stability of investigated compounds was monitored using a Nexera UHPLC system (Shimadzu, Kyoto, Japan) consisting of a CBM-20A controller, two LC-30AD pumps, a DGU-20 A5R degasser, an SPD-M20A photo diode array detector, a CTO-20AC column oven, a SIL-30AC autosampler.

The chromatographic separation was carried out on a Kinetex™ C18 150 × 2.1 mm × 2.6 μm (100 Å) column (Phenomenex, Bologna, Italy). The optimal mobile phase consisted of 0.1 % HCOOH/H_2O v/v (A) and 0.1 % HCOOH/ACN v/v (B). Analysis was performed in gradient elution as follows: 0–14.00 min, 2–85 % B; 14–16.00 min, isocratic to 95 % B; then 5 min for column re-equilibration. Flow rate was 0.5 mL min^{-1}. The column oven temperature was set to 40 °C. Injection volume was 3 μL of each sample. The following PDA parameters were applied: sampling rate, 12.5 Hz; detector time constant, 0.160 s; cell temperature, 40 °C. Data acquisition was set in the range 190–800 nm and chromatograms were monitored at 254 nm.

For the calibration curves, the primary stock solutions were prepared in DMSO. The intermediate stock solutions and the working standard solutions were prepared by serial dilution of the stock solutions in methanol. The calibration curve was obtained in a concentration range of 50–1.0 μM with five concentration levels and triplicate injection of each level were run. Peak areas were plotted against corresponding concentrations and the linear regression was used to generate a calibration curve with R^2 values was ≥0.999.

The method was validated in terms of specificity and selectivity, limits of detection (LOD), limits of quantification (LOQ), accuracy and precision (Table S1). Specificity and selectivity parameters were evaluated by analysing blank matrix samples from different batches to assess

the potential interference of endogenous components in the samples. Chromatograms of these blank matrix samples were compared with chromatograms of matrix samples spiked with a very low concentration of the compound of interest. LOD and LOQ were calculated by using the standard deviation (SD) and the slope of the calibration curve, multiplied by 3.3 and 10, respectively. The repeatability of the chromatographic system was assessed in terms of intra-day and inter-day precision. The accuracy was calculated by the percentage relative error (Er %), and the precision was evaluated by the percentage of relative standard deviation (% RSD). The obtained data demonstrated acceptable accuracy and precision of the developed analytical method.

4.3.2. Drug metabolism studies by HLM

25 μL of 5 mg/mL human microsomes (HLM, Thermo Fisher Scientific, Bremen, Germany) were pre-incubated with 0.625 μL of 100 μg/mL alamethicin, which forms pores in microsomal membranes, promoting access of substrate and cofactor to UGT enzymes. Then 2.5 μL of sample (5 mM) with 168 μL of 100 mM phosphate buffer (pH 7.4), 4 μL of 500 mM magnesium chloride were added, the mixture was incubated at 37 °C for 5 min. The reaction started by adding 50 μL of mix NADPH 10 mM and UDP-GlcUA (uridine diphosphate-glucuronic acid) 20 mM as cofactors (1:1 v/v) and was carried out 37 °C for 30, 60, 90 and 120 min in a Thermomixer comfort (Eppendorf, Hamburg, Germany). The reaction was stopped by the addition of 300 μL ice-cold acetonitrile, and then samples were centrifuged at 14,000 rpm at 25 °C for 5 min (Eppendorf® microcentrifuge 5424, Hamburg, Germany). The supernatants were collected and analyzed in triplicate by UHPLC. The control at 0 min was obtained by the addition of the organic solvent immediately after incubation with microsomes. As the positive control was used testosterone while the negative control was prepared by incubation up to 60 min without UDP-GlcUA/NADPH. The negative control is essential to detect problems such as non-specific protein binding or heat instability.

The extent of metabolism is quantified as a percentage of the parent compound turnover. The results are reported as mean ± standard deviation (SD) from two independent experiments.

The results were expressed in terms of *in vitro* microsome half-lives ($t_{1/2}$), *in vitro* intrinsic clearance ($CLint_{in\ vitro}$) and intrinsic *in vivo* clearance ($CLint_{in\ vivo}$). *In vitro* half-lives ($t_{1/2}$) were calculated using the expression $t_{1/2} = 0.693/b$, where b is the slope found in the linear fit of the natural logarithm of the fraction remaining of the parent compound *vs*. incubation time. Microsomal intrinsic clearance was calculated as $CLint_{in\ vitro} = (1000) \times (0.693/t_{1/2})/0.5$. The intrinsic *in vitro* clearance was scaled to the intrinsic *in vivo* clearance ($CLint_{in\ vivo}$) using human physiology-based scaling factor (PBSF): $CLint_{in\ vivo} = CLint_{in\ vitro} \times PBSF$ (microsome protein/gram liver: 32 × gram liver/kg b.w.: 25.7) [48].

4.4. Biological assays

4.4.1. Cell-free mPGES-1 activity assay

Preparation of mPGES-1 in microsomes of A549 cells and determination of PGE_2 formation under cell-free conditions was performed as previously described [22,23]. In brief, A549 were treated with 1 ng/mL interleukin-1β for 48 h at 37 °C and 5 % CO_2 to induce expression of mPGES-1. After sonification, the homogenate was subjected to differential centrifugation at 10,000 g for 10 min and 174,000 g for 1 h at 4 °C. The pelleted microsomal fraction was resuspended in 1 mL of homogenization buffer (0.1 M potassium phosphate buffer, pH 7.4, 1 mM phenylmethanesulfonyl fluoride, 60 μg/mL soybean trypsin inhibitor, 1 μg/mL leupeptin, 2.5 mM glutathione, and 250 mM sucrose), and the total protein concentration was determined using Bradford protein assay. Microsomal membranes were diluted in potassium phosphate buffer (0.1 M, pH 7.4) containing 2.5 mM glutathione. Test compounds or vehicle were added, and after 15 min at 4 °C, the reaction (100 μL total volume) was initiated by the addition of 20 μM PGH_2 (final concentration). After 1 min at 4 °C, the reaction was terminated using stop solution (100 μL; 40 mM $FeCl_2$, 80 mM citric acid, and 10 μM 11β-PGE_2 as internal standard). Formed PGE_2 was separated by solid-phase extraction and analyzed by RP-HPLC as described previously [23].

4.4.2. Cell-free sEH activity assay

Expression, purification and activity assay of human recombinant sEH were performed as described before [28]. Briefly, Sf9 cells, infected with a recombinant baculovirus, were sonicated (3 × 10 s at 4 °C) in lysis buffer containing $NaHPO_4$ (50 mM, pH 8.0), NaCl (300 mM), glycerol (10 %), EDTA (1 mM), phenyl-methanesulphonylfluoride (1 mM), leupeptin (1 μg/mL), and soybean trypsin inhibitor (60 μg/mL). After centrifugation (100,000 × *g*, 60 min, 4 °C) the supernatants were subjected to benzyl-thiosepharose-affinity chromatography to purify sEH using 4-fluorochalcone oxide in PBS containing DTT (1 mM) and EDTA (1 mM) as elution buffer. Dialyzed and concentrated (Millipore Amicon-Ultra-15 centrifugal filter) sEH was assayed for total protein with Bio-Rad protein detection kit (Bio-Rad Laboratories, Munich, Germany) and the enzyme activity was determined by using a fluorescence-based assay as described before [28]. In brief, sEH was diluted in Tris buffer (25 mM, pH 7.0) supplemented with BSA (0.1 mg/mL) and pre-incubated with test compounds or vehicle (0.1 % DMSO) for 15 min at room temperature. The reaction was started by the addition of 50 mM 3-phenyl-cyano(6-methoxy-2-naphthalenyl)methyl ester-2-oxiraneacetic acid (PHOME), a non-fluorescent compound that is enzymatically converted into fluorescent 6-methoxy-naphtaldehyde at room temperature. After 60 min, the reaction was stopped by $ZnSO_4$ (200 mM) and fluorescence was detected (λ_{em} 465 nm, λ_{ex} 330 nm).

4.5. Preclinical studies in cellular models

4.5.1. Human cell cultures

HCT-116 cells (CCL-247™), an epithelial-like carcinoma cell line derived from the colon of an adult male with colon cancer, were purchased from ATCC (Virginia, USA). The cells were cultured in RPMI medium (Invitrogen, Paisley, UK) supplemented with 10 % fetal bovine serum (FBS, Cambrex, Verviers, Belgium), 2 mM L-glutamine (Sigma, Milan, Italy), 100 units/ml penicillin (Sigma), and 100 μg/mL streptomycin (Sigma). Cultures were maintained in a humidified incubator at 37 °C with 5 % carbon dioxide, following the ATCC guidelines [37].

HaCaT cells, human immortalized keratinocytes (generously provided by Dr. Valeria Cicatiello at the Italian National Research Council (CNR), Institute of Genetics and Biophysics, Naples, Italy), were cultured in a humidified atmosphere with 5 % CO_2 at 37 °C. The cells were grown in DMEM (Invitrogen) supplemented with 10 % fetal bovine serum (FBS, Cambrex), 2 mM L-glutamine, 100 units/mL penicillin (Sigma-Aldrich), and 100 μg/mL streptomycin. Cells were seeded at a density of 2–4 x 10^4 cells/cm^2 and cultured until reaching approximately 80–90 % confluence [49]. HaCaT cells serve as an ideal *in vitro* model for studying biocompatibility and toxicological cellular responses.

4.5.2. Bioscreens in vitro for anticancer activity

The bioactivity and cellular responses to *in vitro* treatment with compounds **7d** and **7e** were assessed using a "cell survival index", which combines cell viability evaluation with cell counting. The cell survival index is calculated as the arithmetic mean of the percentage values derived from the MTT (3-[4,5-dimethylthiazol-2-yl]-2,5 diphenyl tetrazolium bromide) assay and automated cell counting [50]. HCT-116 and HaCaT cells were seeded in 96-well culture plates at a density of 10^4 cells per well and allowed to grow for 24 h. Subsequently, the culture medium was replaced with fresh medium, and the cells were exposed to various concentrations (2.5–50 μM) of the test compounds **7d** and **7e** for an additional 48 h. After treatment, the medium was removed, and the cells were incubated with 20 μL per well of an MTT solution (5 mg/mL MTT, Sigma) for 1 h in a humidified incubator with 5 % CO_2 at 37 °C. The incubation was terminated by removing the MTT solution and adding 100 μL per well of DMSO to solubilize the formazan crystals.

Absorbance was measured at 550 nm using a microplate reader (iMark microplate reader, Bio-Rad, Milan, Italy). Cell numbers were determined using the TC20 automated cell counter (Bio-Rad, Milan, Italy), which employs disposable slides, TC20 trypan blue dye (0.4 % w/v in 0.81 % sodium chloride and 0.06 % potassium phosphate dibasic solution), and a CCD camera to count cells based on image analysis. After removing the medium, the cells were collected, and 10 μL of the cell suspension, mixed with a 0.4 % trypan blue solution at a 1:1 ratio, were loaded into the chambers of the disposable slides. The results were expressed as total cell count (cells/mL). The instrument automatically incorporates the dilution factor and provides both the live cell count and the percentage of viability when trypan blue-stained cells are detected. Total counts and live/dead ratios from random samples of each cell line were compared with manual hemocytometer counts in control experiments. The IC_{50} values were determined from concentration-effect curves obtained by plotting data from six replicates of each experiment, with each experiment repeated four times, resulting in a total of 24 samples ($n = 24$). Nonlinear regression analysis for concentration-effect curves was performed using GraphPad Prism 8.0 software [50].

4.5.3. Statistical data analysis

Data are expressed as mean ± SEM. IC_{50} values were calculated by nonlinear regression using GraphPad Prism Version 8.0 software (San Diego, CA) one site binding competition. Statistical evaluation of the data was performed by one-way ANOVA followed by a Bonferroni post hoc test for multiple comparisons.

CRediT authorship contribution statement

Gianluigi Lauro: Writing – original draft, Validation, Software, Methodology, Investigation, Formal analysis, Conceptualization. **Michela Aliberti:** Writing – original draft, Validation, Software, Methodology, Investigation, Formal analysis. **Mauro De Nisco:** Writing – original draft, Methodology, Investigation, Formal analysis. **Silvana Pedatella:** Writing – original draft, Methodology, Investigation, Formal analysis. **Giacomo Pepe:** Validation, Methodology, Investigation, Formal analysis. **Manuela Giovanna Basilicata:** Methodology, Investigation, Formal analysis. **Maria Giovanna Chini:** Methodology, Investigation, Formal analysis. **Katrin Fischer:** Methodology, Investigation, Formal analysis. **Robert K. Hofstetter:** Validation, Methodology, Investigation, Formal analysis. **Oliver Werz:** Validation, Methodology, Investigation, Formal analysis. **Maria Grazia Ferraro:** Validation, Methodology, Investigation, Formal analysis. **Marialuisa Piccolo:** Validation, Methodology, Investigation, Formal analysis. **Carlo Irace:** Validation, Methodology, Investigation, Formal analysis. **Anella Saviano:** Investigation, Formal analysis. **Pietro Campiglia:** Investigation, Formal analysis. **Alessia Bertamino:** Investigation, Formal analysis. **Carmine Ostacolo:** Investigation, Formal analysis. **Tania Ciaglia:** Investigation, Formal analysis. **Michele Manfra:** Writing – original draft, Supervision, Investigation, Formal analysis. **Giuseppe Bifulco:** Writing – original draft, Supervision, Resources, Methodology, Investigation.

Declaration of competing interest

The authors declare that they have no known competing financial interests or personal relationships that could have appeared to influence the work reported in this paper.

Acknowledgements

This study was supported by AIRC under IG 2018—ID 21397 and IG 2023—ID 28846 projects (Principal Investigator: Bifulco Giuseppe). ASav is supported by RTD-A research contract for the thematic spoke "Validating acid nucleic-based drugs using *in vitro* and *in vivo* models of cancer and immune-related diseases". The research activity is focused on topics of interest for the Department of Pharmacy, Federico II, included in the grant application marked MUR identification code CN00000041 ″National Center for Gene Therapy and Drugs based on RNA Technology" (initiative financed by the European Union – NextGenerationEU and Funding granted with Directorial Decree n.1035 of 06.17.2022 under PNRR MUR – M4C2 – Investment 1.4- CUP UNINA: E63C22000940007).

Appendix. A Supplementary data

Supplementary data to this article can be found online at https://doi.org/10.1016/j.ejmech.2025.117402.

Data availability

Data supporting the conclusions of this work are included in the manuscript or in the Supporting Information. Further data will be made available on request.

References

[1] J. Ke, Y. Yang, Q. Che, F. Jiang, H. Wang, Z. Chen, M. Zhu, H. Tong, H. Zhang, X. Yan, X. Wang, F. Wang, Y. Liu, C. Dai, X. Wan, Prostaglandin E_2 (PGE2) promotes proliferation and invasion by enhancing SUMO-1 activity via EP4 receptor in endometrial cancer, Tumor Biol. 37 (2016) 12203–12211, https://doi.org/10.1007/s13277-016-5087-x.

[2] Y.-Y. Zhang, Y.-D. Yao, J.-F. Luo, Z.-Q. Liu, Y.-M. Huang, F.-C. Wu, Q.-H. Sun, J.-X. Liu, H. Zhou, Microsomal prostaglandin E_2 synthase-1 and its inhibitors: molecular mechanisms and therapeutic significance, Pharmacol. Res. 175 (2022) 105977, https://doi.org/10.1016/j.phrs.2021.105977.

[3] A. Koeberle, S.A. Laufer, O. Werz, Design and development of microsomal prostaglandin E_2 synthase-1 inhibitors: challenges and future directions, J. Med. Chem. 59 (2016) 5970–5986, https://doi.org/10.1021/acs.jmedchem.5b01750.

[4] K.M. Wagner, C.B. McReynolds, W.K. Schmidt, B.D. Hammock, Soluble epoxide hydrolase as a therapeutic target for pain, inflammatory and neurodegenerative diseases, Pharmacol. Ther. 180 (2017) 62–76, https://doi.org/10.1016/J.PHARMTHERA.2017.06.006.

[5] C.B. McReynolds, S.H. Hwang, J. Yang, D. Wan, K. Wagner, C. Morisseau, D. Li, W. K. Schmidt, B.D. Hammock, Pharmaceutical effects of inhibiting the soluble epoxide hydrolase in canine osteoarthritis, Front. Pharmacol. 10 (2019) 533, https://doi.org/10.3389/fphar.2019.00533.

[6] Q. Qu, W. Xuan, G. Fan, Roles of resolvins in the resolution of acute inflammation, Cell Biol. Int. 39 (2015) 3–22, https://doi.org/10.1002/cbin.10345.

[7] G. Lauro, S. Terracciano, V. Cantone, D. Ruggiero, K. Fischer, S. Pace, O. Werz, I. Bruno, G. Bifulco, A combinatorial virtual screening approach driving the synthesis of 2,4-thiazolidinedione-based molecules as new dual mPGES-1/5-LO inhibitors, ChemMedChem 15 (2020) 481–489, https://doi.org/10.1002/cmdc.201900694.

[8] G. Lauro, M. Strocchia, S. Terracciano, I. Bruno, K. Fischer, C. Pergola, O. Werz, R. Riccio, G. Bifulco, Exploration of the dihydropyrimidine scaffold for the development of new potential anti-inflammatory agents blocking prostaglandin E_2 synthase-1 enzyme (mPGES-1), Eur. J. Med. Chem. 80 (2014) 407–415, https://doi.org/10.1016/j.ejmech.2014.04.061.

[9] M.G. Chini, A. Giordano, M. Potenza, S. Terracciano, K. Fischer, M.C. Vaccaro, E. Colarusso, I. Bruno, R. Riccio, A. Koeberle, O. Werz, G. Bifulco, Targeting mPGES-1 by a combinatorial approach: identification of the aminobenzothiazole scaffold to suppress PGE2 levels, ACS Med. Chem. Lett. 11 (2020) 783–789, https://doi.org/10.1021/acsmedchemlett.9b00618.

[10] G. Lauro, M. Manfra, S. Pedatella, K. Fischer, V. Cantone, S. Terracciano, A. Bertamino, C. Ostacolo, I. Gomez-Monterrey, M. De Nisco, R. Riccio, E. Novellino, O. Werz, P. Campiglia, G. Bifulco, Identification of novel microsomal prostaglandin E2 synthase-1 (mPGES-1) lead inhibitors from Fragment Virtual Screening, Eur. J. Med. Chem. 125 (2017) 278–287, https://doi.org/10.1016/j.ejmech.2016.09.042.

[11] E. Colarusso, M. Potenza, G. Lauro, M.G. Chini, V. Sepe, A. Zampella, K. Fischer, R. K. Hofstetter, O. Werz, G. Bifulco, Thiazolidin-4-one-based compounds interfere with the eicosanoid biosynthesis pathways by mPGES-1/sEH/5-LO multi-target inhibition, Eur. J. Med. Chem. Rep 5 (2022) 100046, https://doi.org/10.1016/j.ejmcr.2022.100046.

[12] E. Gazzillo, E. Colarusso, A. Giordano, M.G. Chini, M. Potenza, R.K. Hofstetter, M. Iorizzi, O. Werz, G. Lauro, G. Bifulco, Repositioning of small molecules through the inverse virtual screening *in silico* tool: case of benzothiazole-based inhibitors of soluble epoxide hydrolase (sEH), ChemPlusChem (2024) e202400234, https://doi.org/10.1002/cplu.202400234.

[13] M. Potenza, A. Giordano, M.G. Chini, A. Saviano, C. Kretzer, F. Raucci, M. Russo, G. Lauro, S. Terracciano, I. Bruno, M. Iorizzi, R.K. Hofstetter, S. Pace, F. Maione, O. Werz, G. Bifulco, Identification of 2-Aminoacyl-1,3,4-thiadiazoles as prostaglandin E_2 and leukotriene biosynthesis inhibitors, ACS Med. Chem. Lett. 14 (2023) 26–34, https://doi.org/10.1021/acsmedchemlett.2c00343.

[14] E. Gazzillo, S. Terracciano, D. Ruggiero, M. Potenza, M.G. Chini, G. Lauro, K. Fischer, R.K. Hofstetter, A. Giordano, O. Werz, I. Bruno, G. Bifulco, Repositioning of quinazolinedione-based compounds on soluble epoxide hydrolase (sEH) through 3D structure-based pharmacophore model-driven investigation, Molecules 27 (2022) 3866, https://doi.org/10.3390/molecules27123866.
[15] G. Lauro, V. Cantone, M. Potenza, K. Fischer, A. Koeberle, O. Werz, R. Riccio, G. Bifulco, Discovery of 3-hydroxy-3-pyrrolin-2-one-based mPGES-1 inhibitors using a multi-step virtual screening protocol, MedChemComm 9 (2018) 2028–2036, https://doi.org/10.1039/c8md00497h.
[16] R.S. Mancini, C.J. Barden, D.F. Weaver, M.A. Reed, Furazans in medicinal Chemistry, J. Med. Chem. 64 (2021) 1786–1815, https://doi.org/10.1021/acs.jmedchem.0c01901.
[17] T. Sjögren, J. Nord, M. Ek, P. Johansson, G. Liu, S. Geschwindner, Crystal structure of microsomal prostaglandin E2 synthase provides insight into diversity in the MAPEG superfamily, Proc. Natl. Acad. Sci. U.S.A. 110 (2013) 3806–3811, https://doi.org/10.1073/pnas.1218504110.
[18] D. Li, N. Howe, A. Dukkipati, S.T.A. Shah, B.D. Bax, C. Edge, A. Bridges, P. Hardwicke, O.M.P. Singh, G. Giblin, A. Pautsch, R. Pfau, G. Schnapp, M. Wang, V. Olieric, M. Caffrey, Crystallizing membrane proteins in the lipidic mesophase. Experience with human prostaglandin E_2 synthase 1 and an evolving strategy, Cryst. Growth Des. 14 (2014) 2034–2047, https://doi.org/10.1021/cg500157x.
[19] L.D. Bratton, P.C. Unangst, J.R. Rubin, B.K. Trivedi, Preparation of 6-, 7-, and 8-substituted derivatives of 2-Oxa-1,3,4,10-tetraazacyclopenta[b]fluoren-9-one, J. Heterocycl. Chem. 38 (2001) 1103–1111, https://doi.org/10.1002/jhet.5570380514.
[20] K. Huang, M. Ortiz-Marciales, V. Stepanenko, M. De Jesús, W. Correa, A practical and efficient route for the highly enantioselective synthesis of mexiletine analogues and novel β-thiophenoxy and pyridyl ethers, J. Org. Chem. 73 (2008) 6928–6931, https://doi.org/10.1021/jo801181d.
[21] C. Marminon, A. Nacereddine, Z. Bouaziz, P. Nebois, J. Jose, M. Le Borgne, Microwave-assisted oxidation of indan-1-ones into ninhydrins, Tetrahedron Lett. 56 (2015) 1840–1842, https://doi.org/10.1016/j.tetlet.2015.02.086.
[22] A. Koeberle, U. Siemoneit, U. Bühring, H. Northoff, S. Laufer, W. Albrecht, O. Werz, Licofelone suppresses prostaglandin E2 formation by interference with the inducible microsomal prostaglandin E2 synthase-1, J. Pharmacol. Exp. Therapeut. 326 (2008) 975, https://doi.org/10.1124/jpet.108.139444.
[23] J. Bauer, S. Kuehnl, J.M. Rollinger, O. Scherer, H. Northoff, H. Stuppner, O. Werz, A. Koeberle, Carnosol and carnosic acids from salvia officinalis inhibit microsomal prostaglandin E_2 synthase-1, J. Pharmacol. Exp. Therapeut. 342 (2012) 169–176, https://doi.org/10.1124/jpet.112.193847.
[24] F. Fantasma, V. Samukha, M. Aliberti, E. Colarusso, M.G. Chini, G. Saviano, V. De Felice, G. Lauro, A. Casapullo, G. Bifulco, M. Iorizzi, Essential oils of laurus nobilis L.: from chemical analysis to *in silico* investigation of anti-inflammatory activity by soluble epoxide hydrolase (sEH) inhibition, Foods 13 (2024) 2282, https://doi.org/10.3390/foods13142282.
[25] H.C. Shen, B.D. Hammock, Discovery of inhibitors of soluble epoxide hydrolase: a target with multiple potential therapeutic indications, J. Med. Chem. 55 (2012) 1789–1808, https://doi.org/10.1021/jm201468j.
[26] L. Öster, S. Tapani, Y. Xue, H. Käck, Successful generation of structural information for fragment-based drug discovery, Drug Discov. Today 20 (2015) 1104–1111, https://doi.org/10.1016/j.drudis.2015.04.005.
[27] C. Morisseau, M.H. Goodrow, D. Dowdy, J. Zheng, J.F. Greene, J.R. Sanborn, B. D. Hammock, Potent urea and carbamate inhibitors of soluble epoxide hydrolases, Proc. Natl. Acad. Sci. U. S. A. 96 (1999) 8849–8854, https://doi.org/10.1073/pnas.96.16.8849.
[28] B. Waltenberger, U. Garscha, V. Temml, J. Liers, O. Werz, D. Schuster, H. Stuppner, Discovery of potent soluble epoxide hydrolase (sEH) inhibitors by pharmacophore-based virtual screening, J. Chem. Inf. Model. 56 (2016) 747–762, https://doi.org/10.1021/acs.jcim.5b00592.
[29] N. Hariparsad, R.S. Sane, S.C. Strom, P.B. Desai, *In vitro* methods in human drug biotransformation research: implications for cancer chemotherapy, Toxicol. Vitro 20 (2006) 135–153, https://doi.org/10.1016/j.tiv.2005.06.049.
[30] E.F.A. Brandon, C.D. Raap, I. Meijerman, J.H. Beijnen, J.H.M. Schellens, An update on *in vitro* test methods in human hepatic drug biotransformation research: pros and cons, Toxicol. Appl. Pharmacol. 189 (2003) 233–246, https://doi.org/10.1016/S0041-008X(03)00128-5.
[31] L. Jia, X. Liu, The conduct of drug metabolism studies considered good practice (II): *in vitro* experiments, Curr. Drug Metabol. 8 (2007) 822–829, https://doi.org/10.2174/138920007782798207.
[32] L. Di, E.H. Kerns, Y. Hong, T.A. Kleintop, O.J. Mc Connell, D.M. Huryn, Optimization of a higher throughput microsomal stability screening assay for profiling drug discovery candidates, J. Biomol. Screen 8 (2003) 453–462, https://doi.org/10.1177/1087057103255988.
[33] K.S. Pang, Y.R. Han, K. Noh, P.I. Lee, M. Rowland, Hepatic clearance concepts and misconceptions: why the well-stirred model is still used even though it is not physiologic reality? Biochem. Pharmacol. 169 (2019) 113596 https://doi.org/10.1016/j.bcp.2019.07.025.
[34] C.A. McNaney, D.M. Drexler, S.Y. Hnatyshyn, T.A. Zvyaga, J.O. Knipe, J. V Belcastro, M. Sanders, An automated liquid chromatography-mass spectrometry process to determine metabolic stability half-life and intrinsic clearance of drug candidates by substrate depletion, assay drug, Dev Technol 6 (2008) 121–129, https://doi.org/10.1089/adt.2007.103.
[35] Y. Sasaki, Y. Nakatani, S. Hara, Role of microsomal prostaglandin E synthase-1 (mPGES-1)-derived prostaglandin E_2 in colon carcinogenesis, Prostag. Other Lipid Mediat. 121 (2015) 42–45, https://doi.org/10.1016/j.prostaglandins.2015.06.006.
[36] Y.H. Kim, K.J. Kim, Upregulation of prostaglandin E_2 by inducible microsomal prostaglandin E synthase-1 in colon cancer, Ann Coloproctol 38 (2022) 153–159, https://doi.org/10.3393/ac.2021.00374.0053.
[37] A. Rajput, I. Dominguez San Martin, R. Rose, A. Beko, C. LeVea, E. Sharratt, R. Mazurchuk, R.M. Hoffman, M.G. Brattain, J. Wang, Characterization of HCT116 human colon cancer cells in an orthotopic model, J. Surg. Res. 147 (2008) 276–281, https://doi.org/10.1016/j.jss.2007.04.021.
[38] Schrödinger, Schrödinger Release 2021-1: CombiGlide, Schrödinger, LLC, New York, NY, 2021.
[39] Schrödinger Release 2021-1: QikProp, Schrödinger, LLC, New York, NY, 2021.
[40] Schrödinger Release 2021-1, LigPrep, Schrödinger, LLC, New York, NY, 2021.
[41] Schrödinger Release 2021-1: Protein Preparation Wizard, 2021. Epik, Schrödinger, LLC, New York, NY, 2021; Impact, Schrödinger, LLC, New York, NY; Prime, Schrödinger, LLC, New York, NY.
[42] G. Madhavi Sastry, M. Adzhigirey, T. Day, R. Annabhimoju, W. Sherman, Protein and ligand preparation: parameters, protocols, and influence on virtual screening enrichments, J. Comput. Aided Mol. Des. 27 (2013) 221–234, https://doi.org/10.1007/s10822-013-9644-8.
[43] Schrödinger Release 2021-1: Glide, Schrödinger, LLC, New York, NY, 2021.
[44] R.A. Friesner, R.B. Murphy, M.P. Repasky, L.L. Frye, J.R. Greenwood, T.A. Halgren, P.C. Sanschagrin, D.T. Mainz, Extra precision Glide: docking and scoring incorporating a model of hydrophobic enclosure for Protein−Ligand complexes, J. Med. Chem. 49 (2006) 6177–6196, https://doi.org/10.1021/jm051256o.
[45] T.A. Halgren, R.B. Murphy, R.A. Friesner, H.S. Beard, L.L. Frye, W.T. Pollard, J. L. Banks, Glide: a new approach for rapid, accurate docking and scoring. 2. Enrichment factors in database screening, J. Med. Chem. 47 (2004) 1750–1759, https://doi.org/10.1021/jm030644s.
[46] R.A. Friesner, J.L. Banks, R.B. Murphy, T.A. Halgren, J.J. Klicic, D.T. Mainz, M. P. Repasky, E.H. Knoll, M. Shelley, J.K. Perry, D.E. Shaw, P. Francis, P.S. Shenkin, Glide: a new approach for rapid, accurate docking and scoring. 1. Method and assessment of docking accuracy, J. Med. Chem. 47 (2004) 1739–1749, https://doi.org/10.1021/jm0306430.
[47] Y. Yang, K. Yao, M.P. Repasky, K. Leswing, R. Abel, B.K. Shoichet, S. V Jerome, Efficient exploration of chemical space with docking and deep learning, J. Chem. Theor. Comput. 17 (2021) 7106–7119, https://doi.org/10.1021/acs.jctc.1c00810.
[48] Y. Chen, F. Zhu, J. Hammill, G. Holbrook, L. Yang, B. Freeman, K.L. White, D. M. Shackleford, K.G. O'Loughlin, S.A. Charman, J.C. Mirsalis, R.K. Guy, Selecting an anti-malarial clinical candidate from two potent dihydroisoquinolones, Malar. J. 20 (2021) 107, https://doi.org/10.1186/s12936-021-03617-1.
[49] M.C. Miniaci, C. Irace, A. Capuozzo, M. Piccolo, A. Di Pascale, A. Russo, P. Lippiello, F. Lepre, G. Russo, R. Santamaria, Cysteine prevents the reduction in keratin synthesis induced by iron deficiency in human keratinocytes, J. Cell. Biochem. 117 (2016) 402–412, https://doi.org/10.1002/jcb.25286.
[50] C. Irace, G. Misso, A. Capuozzo, M. Piccolo, C. Riccardi, A. Luchini, M. Caraglia, L. Paduano, D. Montesarchio, R. Santamaria, Antiproliferative effects of ruthenium-based nucleolipidic nanoaggregates in human models of breast cancer *in vitro*: insights into their mode of action, Sci. Rep. 7 (2017) 45236, https://doi.org/10.1038/srep45236.